bioRxiv preprint doi: https://doi.org/10.1101/2022.04.05.487108; this version posted August 9, 2022. The copyright holder for this preprint (which was not certified by peer review) is the author/funder, who has granted bioRxiv a license to display the preprint in perpetuity. It is made available under aCC-BY-NC-ND 4.0 International license.

1

2 **Full title:**

3 Comparative study between radiofrequency-induced and muscimol-induced inhibition of cul-
4 tured networks of cortical neuron

5

6 **Short title:**

7 Radiofrequency-induced vs. muscimol-induced inhibition

8

9 **Authors:**

10 Clément E. Lemercier[1,2], André Garenne[1], Florence Poulletier de Gannes[1], Corinne El
11 Khoueiry[1], Delia Arnaud-Cormos[3,4], Philippe Levêque[3], Isabelle Lagroye[1,5], Yann Percher-
12 ancier[1], Noëlle Lewis[1]

13

14 **Affiliations :**

15 **1** Laboratoire de l'Intégration du Matériau au Système, CNRS UMR 5218, University of Bor-
16 deaux, Talence, France

17 **2** Faculty of Medicine, Institute of Physiology, Department of Systems Neuroscience, Ruhr
18 University Bochum, Bochum, Germany

19 **3** Univ. Limoges, CNRS, XLIM, UMR 7252, 87000 Limoges, France

20 **4** Institut Universitaire de France (IUF), 75005 Paris, France

21 **5** Paris “*Sciences et Lettres*” Research University, Paris, France

22

23 * Corresponding authors

24 E-mail: clement.lemercier@rub.de (CEL)

25 E-mail: noelle.lewis@u-bordeaux.fr (NL)

bioRxiv preprint doi: https://doi.org/10.1101/2022.04.05.487108; this version posted August 9, 2022. The copyright holder for this preprint (which was not certified by peer review) is the author/funder, who has granted bioRxiv a license to display the preprint in perpetuity. It is made available under aCC-BY-NC-ND 4.0 International license.

26 # Abstract

27 Previous studies have shown that spontaneously active cultured networks of cortical neuron
28 grown planar microelectrode arrays are sensitive to radiofrequency (RF) fields and exhibit an
29 inhibitory response more pronounced as the exposure time and power increase. To better un-
30 derstand the mechanism behind the observed effects, we aimed at identifying similarities and
31 differences between the inhibitory effect of RF fields (continuous wave, 1800 MHz) to the γ-
32 aminobutyric acid type A ($GABA_A$) receptor agonist muscimol (MU). Inhibition of the network
33 bursting activity in response to RF exposure became apparent at an SAR level of 28.6 W/kg
34 and co-occurred with an elevation of the culture medium temperature of ~1 °C. Exposure to RF
35 fields preferentially inhibits bursting over spiking activity and exerts fewer constraints on neu-
36 ral network bursting synchrony, differentiating it from a pharmacological inhibition with MU.
37 Network rebound excitation, a phenomenon relying on the intrinsic properties of cortical neu-
38 rons, was observed following the removal of tonic hyperpolarization after washout of MU but
39 not in response to cessation of RF exposure. This implies that hyperpolarization is not the main
40 driving force mediating the inhibitory effects of RF fields. At the level of single neurons, net-
41 work inhibition induced by MU and RF fields occurred with reduced action potential (AP) half-
42 width. As changes in AP waveform strongly influence efficacy of synaptic transmission, the
43 narrowing effect on AP seen under RF exposure might contribute to reducing network bursting
44 activity. By pointing only to a partial overlap between the inhibitory hallmarks of these two
45 forms of inhibition, our data suggest that the inhibitory mechanisms of the action of RF fields
46 differ from the ones mediated by the activation of $GABA_A$ receptors.

47

bioRxiv preprint doi: https://doi.org/10.1101/2022.04.05.487108; this version posted August 9, 2022. The copyright holder for this preprint (which was not certified by peer review) is the author/funder, who has granted bioRxiv a license to display the preprint in perpetuity. It is made available under aCC-BY-NC-ND 4.0 International license.

48 # Introduction

49 Radiofrequencies are electromagnetic waves ranging from 300 kHz to 300 GHz widely used in
50 modern telecommunication technology. The rapid and continuous increase of environmental
51 man-made RF electromagnetic fields (EMF) has raised concerns about their potential risks on
52 human health. In particular, a large body of research has investigated the possible effects of
53 exposure to RF fields used by mobile phones (300-3000 MHz) on the human central nervous
54 system (CNS) (for reviews see [1-3]). Although evidence exists pointing to an effect of RF
55 fields on brain oscillations [4-7] (reviewed in [8]), evoked potentials [9-10] (but see [11]), and
56 glucose metabolism [12], such changes have not been claimed as having any adverse health
57 effects [13-14]. Interaction between RF fields and biological systems are best understood from
58 a thermal perspective [15-16]. However, compelling evidence suggests that RF fields may also
59 interact with biological systems by producing so-called non-thermal effects (for reviews see
60 [17-19], although see [20-21] for critical reviews), but so far no mechanisms or molecular tar-
61 gets have been identified. Understanding the biological mechanism of non-thermal effects of
62 RF fields on the CNS is not only critical in promoting safety but also holds the promise of useful
63 insights for the development of future biomedical and biotechnological applications.

64 Early research on various neural preparations reported electrophysiological change in response
65 to RF fields [22-26]. Since then, investigations most frequently indicate that RF fields cause
66 neural activity to decrease [27-35] (but see [24, 36-38]), although the nature of the observed
67 effects might depend on the frequency bands to which the neural preparation is exposed (for
68 example see [28, 38]). In recent years, our laboratory has developed an experimental setup al-
69 lowing exposing spontaneously active cultures of cortical neurons grown on a planar microe-
70 lectrode array (MEA) to RF fields, and simultaneously recording the effects [39]. The results
71 obtained with this system indicate that network bursting activity decreases when exposed to RF

bioRxiv preprint doi: https://doi.org/10.1101/2022.04.05.487108; this version posted August 9, 2022. The copyright holder for this preprint (which was not certified by peer review) is the author/funder, who has granted bioRxiv a license to display the preprint in perpetuity. It is made available under aCC-BY-NC-ND 4.0 International license.

72 fields [27] and that the inhibitory response is a function of exposure time and power [28]. Ex-
73 periments done with equivalent thermal heating suggested that the inhibitory effects of RF
74 fields may originate in part from non-thermal interaction with the nervous tissues. However,
75 the mechanism of action of RF fields on neural networks has remained elusive.
76 In the present study, we have aimed to contribute to the understanding of the mechanisms of
77 action behind the inhibitory effects of RF fields on cultured cortical neural networks by per-
78 forming a direct comparison with the inhibitory effects of the $GABA_A$ receptor agonist, musci-
79 mol (MU). The $GABA_A$ receptor is the major inhibitory neurotransmitter receptor responsible
80 for fast inhibition in the mammalian brain [40-41]. Signaling at this receptor is well understood,
81 thus making it a solid reference for comparative studies aiming to infer potential mechanisms
82 of action of particular drugs or treatments. Experiments have been carried out on a new MEA
83 device with improved stability during EMF exposure [42] wherein changes in spiking, bursting
84 activity and action potential (AP) waveform in response to RF fields or MU were analyzed and
85 compared. This comparative approach allowed us to identify similarities and differences be-
86 tween these two forms of inhibition and to employ them as a basis for unravelling a potential
87 mechanism of action of the inhibitory effect of RF fields on cultured neural networks.
88

89 Materials and methods

90 Animals

91 Primary cultures of neocortical neurons were prepared from embryos of gestating Sprague-
92 Dawley rats (Charles River Laboratories, L'Arbresle, France). Experiments involved six ges-
93 tating rats. All procedures were carried out in compliance with the European Community Coun-
94 cil Directive for the Care and Use of laboratory animals (2010/63/EU) and protocols were ap-
95 proved by the Bordeaux Ethics Committee for Animal Experimentation (CEEA - 050).
96

bioRxiv preprint doi: https://doi.org/10.1101/2022.04.05.487108; this version posted August 9, 2022. The copyright holder for this preprint (which was not certified by peer review) is the author/funder, who has granted bioRxiv a license to display the preprint in perpetuity. It is made available under aCC-BY-NC-ND 4.0 International license.

Preparation of primary neural culture

Preparation of primary neural cultures was carried out using the methods described in [27-28]. In brief, under anesthetics (5% isoflurane), gestating rats were euthanized by cervical dislocation, embryos (at embryonic day 18) were collected, and their cortices were dissected and treated with a papain-based dissociation system (Worthington Biochemical, Lakewood, CO, USA). Following mechanical dissociation and two steps of centrifugation (the second with an albumin-inhibitor solution), the pellet containing cortical cells (glial cells and neurons) was resuspended in a neurobasal culture medium (NBM) supplemented with 2% B-27, 1% GlutaMAX, and 1% penicillin-streptomycin (Fisher Scientific, Illkirch, France). The recording chips of autoclaved MEAs (Multi Channel Systems MCS GmbH, Reutlingen, Germany) previously coated with polylysine and laminin (Sigma-Aldrich, St. Quentin-Fallavier, France) were plated with a drop of cellular suspension containing 10^5 cells. Cells were left to sediment and adhere on the MEA chip for up to 2 h and the MEA chambers were then filled with 1 mL of NBM. MEAs were kept in individual petri dishes at 37 °C in a humidified incubator with 5% CO_2 until mature neural network development. Culture mediums were half-exchanged every 48 h until taking recordings.

New MEA design and characteristics

In the present study, a modified version [42] of a 60-channel planar MEA introduced in [39] was used. This new design shared the main characteristic of such MEAs, namely the amplifier contact pads placed underneath the printed circuit board, but presented as main evolutions a reduced chip aperture to the limits of the recording zone and several ground planes in the multi-layered PCB. These evolutions allowed this device to be steadier in terms of Specific Absorption Rate (SAR) and temperature stability during EMF exposure. Indeed, extensive numerical and experimental dosimetry was carried out to assess SAR values and temperature variation on

bioRxiv preprint doi: https://doi.org/10.1101/2022.04.05.487108; this version posted August 9, 2022. The copyright holder for this preprint (which was not certified by peer review) is the author/funder, who has granted bioRxiv a license to display the preprint in perpetuity. It is made available under aCC-BY-NC-ND 4.0 International license.

122 this new MEA. Although it has been noted that SAR values varied slightly within the culture
123 medium with peak SAR values observed in the vicinity of the electrode tips , microscopic tem-
124 perature measurements at the electrodes and exposed neurons level did not show any evidence
125 of local temperature hot spots (see [42] for more details on the numerical and experimental
126 dosimetry of the device). In this modified MEA, SAR values normalized per 1 Watt of incident
127 power were estimated at 5.5 ± 2.3 W/kg.
128

129 Electrophysiology and exposure system

130 The experimental setup for simultaneous electrophysiological recordings and exposure to RF
131 fields or pharmacological agents comprised an MEA coupled to an open transverse electromag-
132 netic cell (TEM) [39, 42-43] and a perfusion system allowing continuous fresh medium ex-
133 change with minimal disturbance. RF signal (CW) at 1800 MHz was delivered to the open TEM
134 cell with a signal generator-amplifier (RFPA, Artigues-près-Bordeaux, France). To enable sim-
135 ultaneous recording and exposure to RF fields, MEAs were maintained “sandwiched“ between
136 the TEM bottom plate and the preamplifier (MEA1060-Inv, MCS GmbH), as described in ear-
137 lier publications [27-28, 39, 42]. Once installed on the MEA amplifier, a perfusion holder
138 (MEA-MEM-PL5, ALA Scientific Instruments Inc., Farmingdale, NY, USA) was inserted into
139 the MEA chamber. Perfusion of fresh culture medium was controlled with a peristaltic pump
140 (REGLO ICC, Hugo Sachs Elektronik, March-Hugstetten, Germany) and the optimal perfusion
141 rate (causing minimal disturbance to neural cultures) was set at ~350 μL/min. In these condi-
142 tions, culture medium was fully exchanged in ~2:50 min. Prior to starting the experiment, cul-
143 tures were allowed to acclimatize to the continuous medium exchange for ~30 min. Recordings
144 were performed in a dry incubator at 37 °C with 5% CO_2. Preamplification gain was 1200 and
145 signals were acquired and digitized at 10 kHz/channel with an MCS-dedicated data acquisition
146 board (MC_Card, MCS GmbH). Signals were recorded and visualized with the MC Rack (MCS

bioRxiv preprint doi: https://doi.org/10.1101/2022.04.05.487108; this version posted August 9, 2022. The copyright holder for this preprint (which was not certified by peer review) is the author/funder, who has granted bioRxiv a license to display the preprint in perpetuity. It is made available under aCC-BY-NC-ND 4.0 International license.

147 GmbH) software. After 30 min of baseline recording, neural cultures were exposed for 15 min
148 either to a sham treatment (SH), a pure continuous carrier radiofrequency (RF) at 1800 MHz,
149 or to the $GABA_A$ receptor agonist muscimol (MU), (Tocris Bioscience, Bristol, UK). After
150 treatment, post-treatment activity was continuously monitored for 45 min. Data from cultures
151 aged between 17 and 27 days in vitro (DIV) were included in the present study (DIV, Median
152 = 20, Interquartile range, IQR = 4.5, n = 35, all experimental groups collapsed).
153

154
Data analysis and metrics

155 Processing and analysis of multi-channel data were performed with the software package
156 SPYCODE [44] developed in MATLAB environment (The MathWorks, Inc., Natick, MA,
157 USA). After signal filtering (Butterworth high-pass filter with a cut-off frequency at 70 Hz),
158 spike detection was performed using the differential threshold precision timing spike detection
159 (PTSD) method described by [45] and spike trains were analyzed for burst detection using the
160 method described by [46]. Changes in neural networks activity in response to 15 min of SH,
161 RF or MU exposure were assessed at the level of the entire MEA by pooling data from all active
162 channels (i.e. showing both spiking and bursting activities). Burst detection was used to com-
163 pute the mean bursting rate (MBR), mean interburst interval (IBI), mean burst duration (BD),
164 mean intraburst spike rate (IBSR), and crossed analysis between burst periods and spike trains
165 allowed computing the mean spiking rate (MSR) for spikes occurring outside bursts. Effects of
166 RF and MU exposure were compared in respect to the SH group after data normalization re-
167 flecting the average fractional variation (R) of a metric (M) during the exposure phase (M_{Expo-}
168 $_{sure}$) relative to the baseline reference phase ($M_{Baseline}$).

169
$$R_M = M_{Exposure}/M_{Baseline} \qquad (1)$$

170 The level of synchronicity for descriptors of bursting activity across MEA channels was eval-
171 uated with the coefficient of variation (CV) defined as the ratio (expressed in %) of the average

bioRxiv preprint doi: https://doi.org/10.1101/2022.04.05.487108; this version posted August 9, 2022. The copyright holder for this preprint (which was not certified by peer review) is the author/funder, who has granted bioRxiv a license to display the preprint in perpetuity. It is made available under aCC-BY-NC-ND 4.0 International license.

172 channel standard deviation to the metric mean value (either IBI, BD or IBSR). The lower the
173 CV, the higher synchronization across MEA channels [47-48]. Inter-channel variation for MBR
174 and MSR relative to the overall average fractional variation (i.e. entire MEA) was used to de-
175 scribe the spatial variability of the effects associated with the treatment. This measure was eval-
176 uated by computing the normalized root mean square error (*Norm. RMSE*) as follow:

177
$$Norm.RMSE = \frac{\sqrt{\sum_{k=1}^{K}(Y - y_k)^2}}{K.Y} \qquad (2)$$

178 Where *'Y'* is the averaged normalized value of MBR or MSR over all MEA channels (*K*) and
179 '*y'* is the averaged normalized value of MBR or MSR at the level of the individual channel (*k*).
180 For example, a *Norm. RMSE* value equal to 0.5 indicates that the mean inter-channel variation
181 to the mean is of 50 %. Computation methods for the metrics described above are reported in
182 S1 Table.
183

184 ## AP sorting and waveform analysis

185 AP detection and sorting were performed with the Offline Sorter V3 (Plexon Inc., Dallas, TX,
186 USA) software over a period of 30 min including 15 min of baseline (pre-exposure phase im-
187 mediately prior to treatment) and 15 min when neural cultures are continuously exposed to the
188 treatment. To ensure reliable sorting between the two recording phases, pre-exposure and ex-
189 posure phases were merged into a single file with the MC_dataTool (MCS GmbH) software.
190 Detection threshold was set at five times the standard deviation of the channel noise level and
191 waveform sample-wide containing single event was set at 4 ms (40 sample, 0.8 ms before peak
192 and 3.2 ms after peak). Note that this method of detection differs from the one used in
193 SPYCODE. AP sorting was performed using the T-Dist E-M method (Outlier Threshold 1.5;
194 D.O.F. Mult. 8) and analyses were executed in batch mode. This method enabled detecting on
195 average 67, 991 ± 10,655 (Mean ± SEM) APs per MEA and to sort on average 40,135 ± 6,114

bioRxiv preprint doi: https://doi.org/10.1101/2022.04.05.487108; this version posted August 9, 2022. The copyright holder for this preprint (which was not certified by peer review) is the author/funder, who has granted bioRxiv a license to display the preprint in perpetuity. It is made available under aCC-BY-NC-ND 4.0 International license.

196 APs per MEA (S1A Fig, data over 15 min during pre-exposure phase from 15 cultures of the
197 RF group used here as representative). Unsorted APs were not analyzed. Hierarchical clustering
198 of the sorted APs indicated that MEA channels presented several sources of AP that were qual-
199 ified either as major (MAJ), auxiliary (AUX) or minor (MIN) contributors to the total number
200 of sorted spikes (S1A and S1B Figs). On average, MAJ, AUX and MIN AP clusters were re-
201 spectively observed in 85.3 ± 3.6, 28 ± 4.5, 12.3 ± 1.8 % of the MEA channels and enclosed
202 respectively on average 68 ± 4.4, 21.4 ± 2.5, 10.6 ± 3.3 % of the total amount of sorted APs
203 (S1A Fig). Comparison of the AP timestamps with the burst periods indicated for the MAJ AP
204 cluster that sorted APs inside bursts ($_{AP}$IB) were roughly twice as numerous (~1.9) as sorted
205 APs outside bursts ($_{AP}$OB) and that this proportion decreased to ~1.3 and ~1.1 respectively for
206 the AUX and MIN AP clusters (S1A Fig). As ~89% of the total amount of sorted APs were
207 enclosed in the MAJ and AUX AP clusters, only waveforms from these two clusters were ana-
208 lyzed. The following were measured from these waveforms - peak, anti-peak amplitude, full
209 width at half maximum (FWHM, through linear interpolation), maximum slope of the rising
210 edge and falling edge. Data from MAJ and AUX clusters were then averaged to reflect the
211 overall change in AP waveform in response to the various treatments. Metrics used to quantify
212 changes in AP waveforms are illustrated in S1C Fig and defined in S3 Table.

213

214 ## Statistics

215 Statistical analysis was performed using the R software [49] and the 'PMCMRplus' library [50].
216 Unless stated, data in the text and supporting information are reported as median and interquar-
217 tile ranges (IQR, .i.e. the differences between Q3 and Q1). To evaluate changes relative to the
218 baseline, raw values at baseline for the different metrics showed in Figs 2 and 5 are reported
219 respectively in tabulated form in S2 and S4 Tables. A Kruskal-Wallis test, followed by a
220 Conover's multiple comparison test, was used to compare differences between groups. A *p*-

bioRxiv preprint doi: https://doi.org/10.1101/2022.04.05.487108; this version posted August 9, 2022. The copyright holder for this preprint (which was not certified by peer review) is the author/funder, who has granted bioRxiv a license to display the preprint in perpetuity. It is made available under aCC-BY-NC-ND 4.0 International license.

221 value < 0.05 was considered statistically significant. Effect size (epsilon-squared, ε^2), when
222 reported, was calculated with the “rcompanion” [51] R package. Data were plotted with the
223 ‘ggplot2’ [52] and ‘ggpubr’ [53] R packages. The compact letter representation method [54]
224 was used to denote statistical significance after pairwise comparisons with the R package
225 ‘multcompView’ [55]. Pairwise comparisons sharing a common letter are not statistically dif-
226 ferent but, on the contrary, the ones not sharing any letter are statistically different.
227

228 # Results

229 ## Dose response relationship between RF- and MU-induced inhibi-
230 tion

231 A photograph of the setup illustrating the different parts is shown in Fig 1A. Heating of the
232 culture medium in response to RF exposure at different SAR levels (range: ~4.8 to ~37.9 W/kg)
233 was measured with a fiber optic probe (Luxtron One, Lumasense Technologies, Milpitas, CA,
234 USA; ± uncertainty 0.1 °C) (Fig 1B) immersed in the culture medium under continuous medium
235 exchange (flow rate ~350 µL/min). After 15 min of exposure, heating peaks ranged from ~0.2
236 to ~1.5 °C respectively for minimum (~4.8 W/kg) and maximum (~37.9 W/kg) tested SAR
237 levels. As cultured networks of cortical neurons are sensitive to RF fields in a dose dependent
238 manner [28], the response relationship between MBR and exposure levels was re-evaluated for
239 the new MEA device used in the present study. With this new type of MEA, inhibition of burst-
240 ing activity became visible for exposure levels over ~25 W/kg and a reduction of ~50 % in
241 MBR was estimated at ~28.6 W/kg (Fig 1C). At this SAR level, reduction of bursting activity
242 after 15 min of exposure co-occurred with an elevation of the medium temperature of ~1 °C.
243 To compare the effects of RF exposure with those of the $GABA_A$ receptor agonist MU under
244 similar levels of inhibition, the relation between MBR and MU concentration was first evalu-

bioRxiv preprint doi: https://doi.org/10.1101/2022.04.05.487108; this version posted August 9, 2022. The copyright holder for this preprint (which was not certified by peer review) is the author/funder, who has granted bioRxiv a license to display the preprint in perpetuity. It is made available under aCC-BY-NC-ND 4.0 International license.

245 ated (Fig 1D). MU exerts a profound inhibitory action on the activity of cultured cortical net-
246 works and its half-maximal inhibitory concentration for the metric MBR ($IC_{50\text{-}MBR}$) was esti-
247 mated to be ~0.25 µM, a value in agreement with other studies on basic receptor and neural
248 culture pharmacology [47, 55-58].

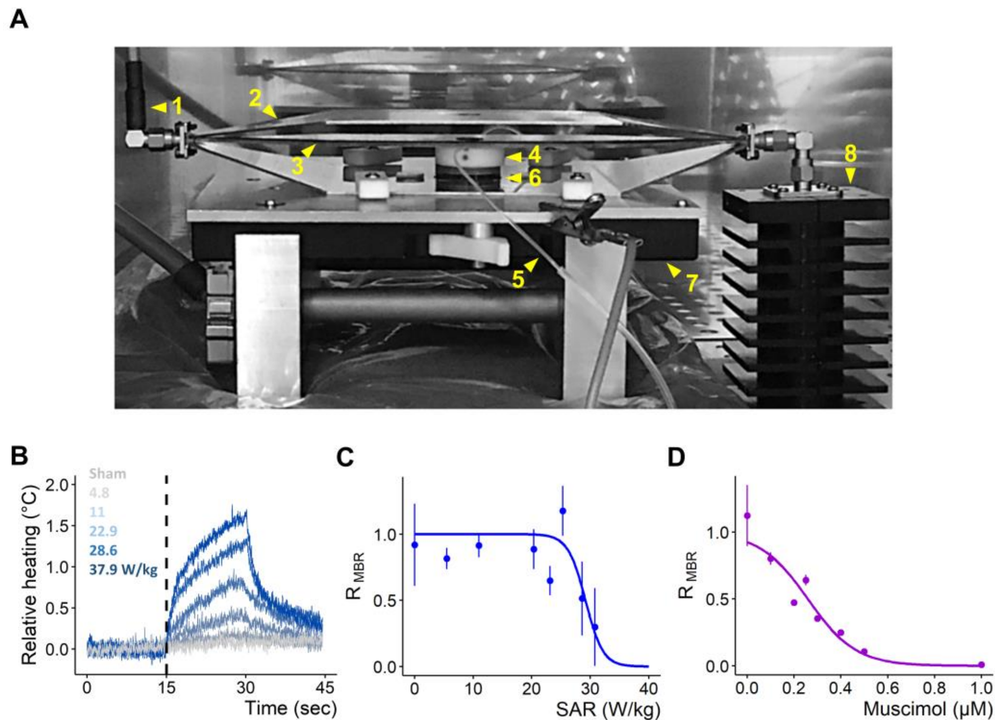

Fig 1. Setup configuration and dose response profile of MBR against SAR level and MU concentration. (A) Photograph of the setup configuration used for simultaneous recording on MEA and exposure to RF fields and pharmacological agents. (1) Coaxial cable connecting an RF-generator/amplifier (located outside the incubator) to (2) an open transverse electromagnetic (TEM) cell. (3) TEM cell septum. (4) Perfusion holder inserted on top of the MEA chamber. (5) Perfusion microtubes for medium exchange. (6) MEA "sandwiched" between TEM bottom ground plate and amplifier ground plate. (7) Inverted MEA preamplifier connected to a MC_Card of a desktop computer. (8) 50 Ω Terminator. **(B)** Relative heating response of the culture medium over 15 min as a function of different SAR levels (W/kg). **(C)** Dose-response relationship between SAR and MBR; results from 21 recordings (18 cultures), 0 (W/kg): n = 21; 5.5: n = 2; 11: n = 3; 20.35: n = 2; 23.1: n = 3; 25.3: n = 3; 28.6: n = 5; 30.6: n = 3. **(D)** Dose-response relationship between MU concentration and MBR; results from 14 recordings (3 cultures), $1e^{-4}$ (µM): n = 2; 0.1: n = 3; 0.2: n = 1; 0.25: n = 2; 0.3: n = 1; 0.4: n = 1; 0.5: n = 2; 1: n = 2. (C-D) Normalized MBR, ratio of the exposure phase to baseline, data shown as Median ± SD. Fits computed with non-linear least squares method, Pearson's Goodness-of-Fit: $p < 0.05$.

249

bioRxiv preprint doi: https://doi.org/10.1101/2022.04.05.487108; this version posted August 9, 2022. The copyright holder for this preprint (which was not certified by peer review) is the author/funder, who has granted bioRxiv a license to display the preprint in perpetuity. It is made available under aCC-BY-NC-ND 4.0 International license.

250 ## RF and MU differentially impacted network activity patterns

251 The inhibitory effects of RF fields and MU were then compared with respect to an SH group
252 after data normalization (see materials and methods). Definitions of the metrics used to describe
253 changes in network activity in Fig 2 are reported in S1 Table. To assess the magnitude of the
254 reported normalized effects with respect to the raw data, raw data at baseline relative to Fig 2
255 are tabulated in S2 Table.

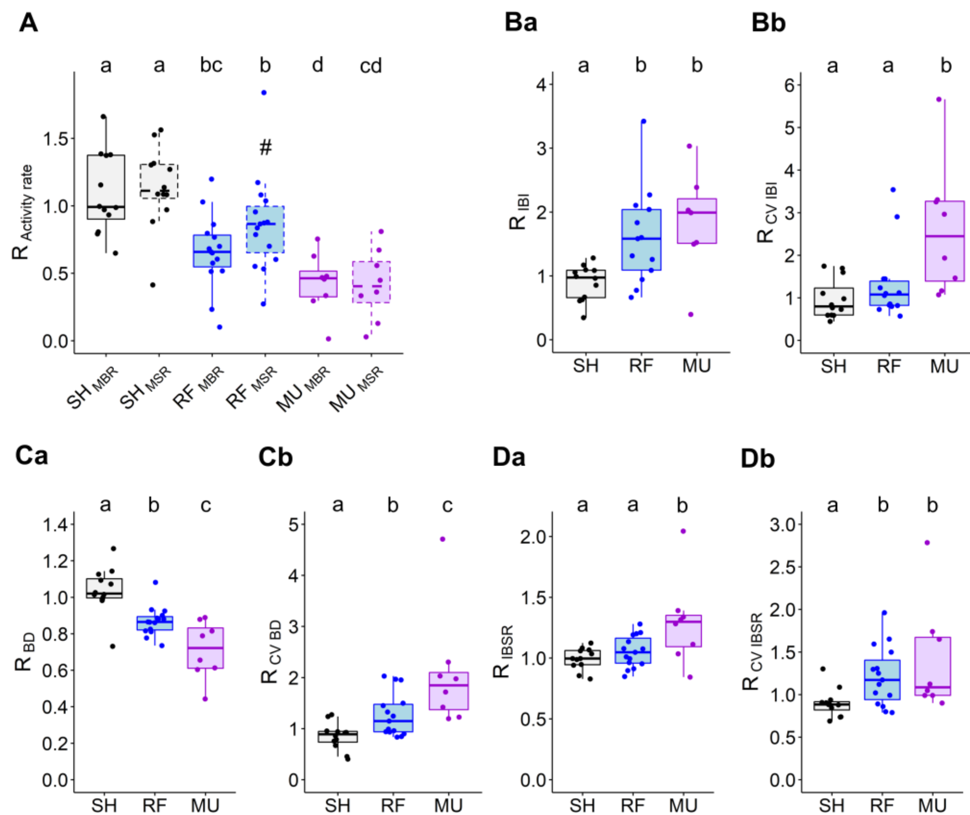

Fig 2. Comparison between RF and MU-induced inhibition of cultured cortical network. (A) Average effect of 15 min of exposure to RF and MU on MBR and MSR (spike outside burst periods). Boxplots with dashed box denote MSR data. (#) is indicative of $p = 0.0535$ against RF_{-MBR} and RF_{-MSR}. **(Ba)** Average effect of 15 min of exposure to RF and MU on mean inter-burst interval (IBI), **(Ca)** mean burst duration (BD), **(Da)** mean inter-burst spike rate (IBSR). (Bb, Cb and Db) Coefficients of variation (CV) respectively for IBI, BD and IBSR. Normalized data, ratio of the exposure phase to baseline. SH: n = 12; RF: n = 15; MU: n = 8. (A-Db). Lower case letters indicate significant differences between groups.

256

257 Exposure to RF fields (SAR of 28.6 W/kg) or MU (0.25 µM) both reduced MBR (RF: ~35%
258 reduction, SH/RF, $p < 0.001$; MU: ~57% reduction, SH/MU, $p < 0.001$) and MSR (RF: ~14%

bioRxiv preprint doi: https://doi.org/10.1101/2022.04.05.487108; this version posted August 9, 2022. The copyright holder for this preprint (which was not certified by peer review) is the author/funder, who has granted bioRxiv a license to display the preprint in perpetuity. It is made available under aCC-BY-NC-ND 4.0 International license.

259 reduction, SH/RF, $p < 0.001$; MU: ~58% reduction, SH/MU, $p < 0.001$). Inhibitory effects of
260 MU on bursting and spiking activities were on average stronger than for RF exposure (RF_{-MBR}/MU_{-MBR}, $p = 0.0412$; RF_{-MSR}/MU_{-MSR}, $p < 0.001$ - Fig 2A). In comparison to MU, RF fields
262 showed a tendency to preferentially inhibit bursting over spiking activity whereas MU reduced
263 equivalently both types of activity (RF_{-MBR}/RF_{-MSR}, $p = 0.0543$, $\varepsilon^2_{RF\text{-}MBR} = 0.387$, $\varepsilon^2_{RF\text{-}MSR} = 0.267$; MU_{-MBR}/ MU_{-MSR}, $p = 0.9057$, $\varepsilon^2_{MU\text{-}MBR} = 0.692$, $\varepsilon^2_{MU\text{-}MSR} = 0.607$).
265 Inhibition of neural network activity was evaluated in the spatial domain by quantifying the
266 inter-channel variability of MBR and MSR variations across all channels of the MEA layout by
267 computing the normalized root mean square error (Norm. RMSE, see materials and methods).
268 Intrinsic variations of this measurement observed in response to SH exposure indicated on av-
269 erage that the level of spatial variability for MBR was slightly lower than for MSR (SH_{-MBR} = 0.22 (0.14); SH_{-MSR} = 0.37 (0.30); $p = 0.0327$). RF- and MU-induced inhibition were both as-
271 sociated with a comparable level of spatial variation of bursting activity across the MEA chan-
272 nels (RF = 0.20 (0.22); MU = 0.28 (0.12); $p = 0.3059$). The degree of spatial variability in MBR
273 was not different from the intrinsic spatial variability observed in response to SH exposure ($p = 0.3024$). In the same way as for the data for MBR, the data for MSR indicated that RF- and
275 MU-induced inhibition caused spiking activity to vary equivalently in space (RF = 0.54 (0.16);
276 MU = 0.65 (0.21); $p = 0.1848$) but spatial fluctuations of MSR were higher than for the intrinsic
277 variation observed with SH exposure ($p = 0.0037$, pooled MSR data across RF and MU); alt-
278 hough as in SH exposure, spatial variations of MBR were lower than for MSR ($p < 0.001$).
279 Collectively these data indicate that RF-induced inhibition occurred within the MEA space as
280 diffusely as the pharmacological inhibition induced by MU.
281 Comparison between RF- and MU-induced inhibitions was pursued with descriptors of bursting
282 activity such as IBI, BD and IBSR and their respective indicators of synchronization across
283 MEA channels with the coefficient of variation (CV, see materials and methods and metrics

bioRxiv preprint doi: https://doi.org/10.1101/2022.04.05.487108; this version posted August 9, 2022. The copyright holder for this preprint (which was not certified by peer review) is the author/funder, who has granted bioRxiv a license to display the preprint in perpetuity. It is made available under aCC-BY-NC-ND 4.0 International license.

284 definition in S1 Table). In response to RF and MU, bursting activity becomes increasingly
285 sparse, as seen by increased IBI (SH/RF, $p = 0.0020$, SH/MU, $p < 0.001$; RF/MU, $p = 0.4528$ -
286 Fig 2Ba). Compared to RF exposure, the inhibitory action of MU was accompanied by a desyn-
287 chronization of bursting activity across MEA channels as seen by an increased CV IBI (SH/RF,
288 $p = 0.2318$; SH/MU, $p < 0.001$; RF/MU , $p = 0.0098$ - Fig 2Bb). RF and MU both decreased
289 BD (SH/RF, $p < 0.001$; SH/MU, $p < 0.001$; RF/MU, $p = 0.0178$ - Fig 2Ca) and desynchronized
290 BD across MEA channels (CV BD: SH/RF, $p = 0.0035$, SH/MU, $p < 0.001$ - Fig 2Cb) but this
291 effect was of a higher magnitude for MU (RF/MU, $p = 0.0128$). MU, but not RF exposure,
292 increased IBSR (SH/RF, $p = 0.2919$; SH/MU, $p = 0.0069$; RF/MU, $p = 0.0476$ - Fig 2Da).
293 However, both treatments desynchronized IBSR across MEA's channels (CV IBSR: SH/RF, p
294 $= 0.0062$; SH/MU, $p = 0.0042$; RF/MU, $p = 0.5388$ - Fig 2Db).
295

296 Differential effect of RF and MU on neural networks temporal ac- 297 tivity pattern

298 Analysis and comparison of the two forms of inhibition were pursued in the temporal domain
299 by measuring bursting rate (BR) and spiking rate (SR) over time (Fig 3). In response to RF or
300 MU, BR dramatically decreased by about half of the baseline level within the first minute fol-
301 lowing exposure (Fig 3A). Similarly to BR, SR reduced within the first minute following ex-
302 posure onset but, in contrast to MU, the latter appeared on average to be less affected by RF
303 fields (Fig 3B). Quantification of the rate of BR inhibition during the initial phase of exposure
304 (initial inhibitory rate, see metrics definition in S1 Table) indicated that RF fields and MU both
305 impacted BR with an equivalent initial potency (SH/RF, $p < 0.001$; SH/MU, $p = 0.0035$;
306 RF/MU, $p = 0.9243$ - Fig 3C). The initial inhibitory rate for SR in response to RF exposure
307 showed a greater level of variability than for BR and was no different from SH (SH/RF, $p =$
308 0.1741 - Fig 3C). On the other hand, MU inhibited BR and SR with an equivalent initial potency

bioRxiv preprint doi: https://doi.org/10.1101/2022.04.05.487108; this version posted August 9, 2022. The copyright holder for this preprint (which was not certified by peer review) is the author/funder, who has granted bioRxiv a license to display the preprint in perpetuity. It is made available under aCC-BY-NC-ND 4.0 International license.

309 (SH_{SR}/MU_{SR}, $p < 0.001$; MU_{BR}/MU_{SR}, $p = 0.6850$ - Fig 3C). Following the initial action of
310 the treatments, BR and SR showed a tendency for a slight regain of activity, although this effect
311 was more marked for MU. In response to washout of MU, a dramatic short-lasting regain of
312 activity of about 1 min was observed. This phenomenon qualified as a postinhibitory rebound
313 (PIR, see metrics definition in S1 Table) was, on average, visible both for BR and SR (Figs 3A
314 and 3B) but only significantly detected for bursting activity (SH_{PIR-BR}/ MU_{PIR-BR} , $p = 0.0128$;
315 SH_{PIR-SR} / MU_{PIR-SR}, $p = 0.0549$ - Fig 3D). Interestingly, PIR was not observed in response to
316 RF exposure cessation (SH_{PIR-BR} / RF_{PIR-BR}, $p = 0.8420$; SH_{PIR-SR} / RF_{PIR-SR}, $p = 0.9821$ - Fig
317 3D). Successive recording phases indicated that neuronal network activity fully recovered from
318 treatment and temporally evolved similarly to SH.

bioRxiv preprint doi: https://doi.org/10.1101/2022.04.05.487108; this version posted August 9, 2022. The copyright holder for this preprint (which was not certified by peer review) is the author/funder, who has granted bioRxiv a license to display the preprint in perpetuity. It is made available under aCC-BY-NC-ND 4.0 International license.

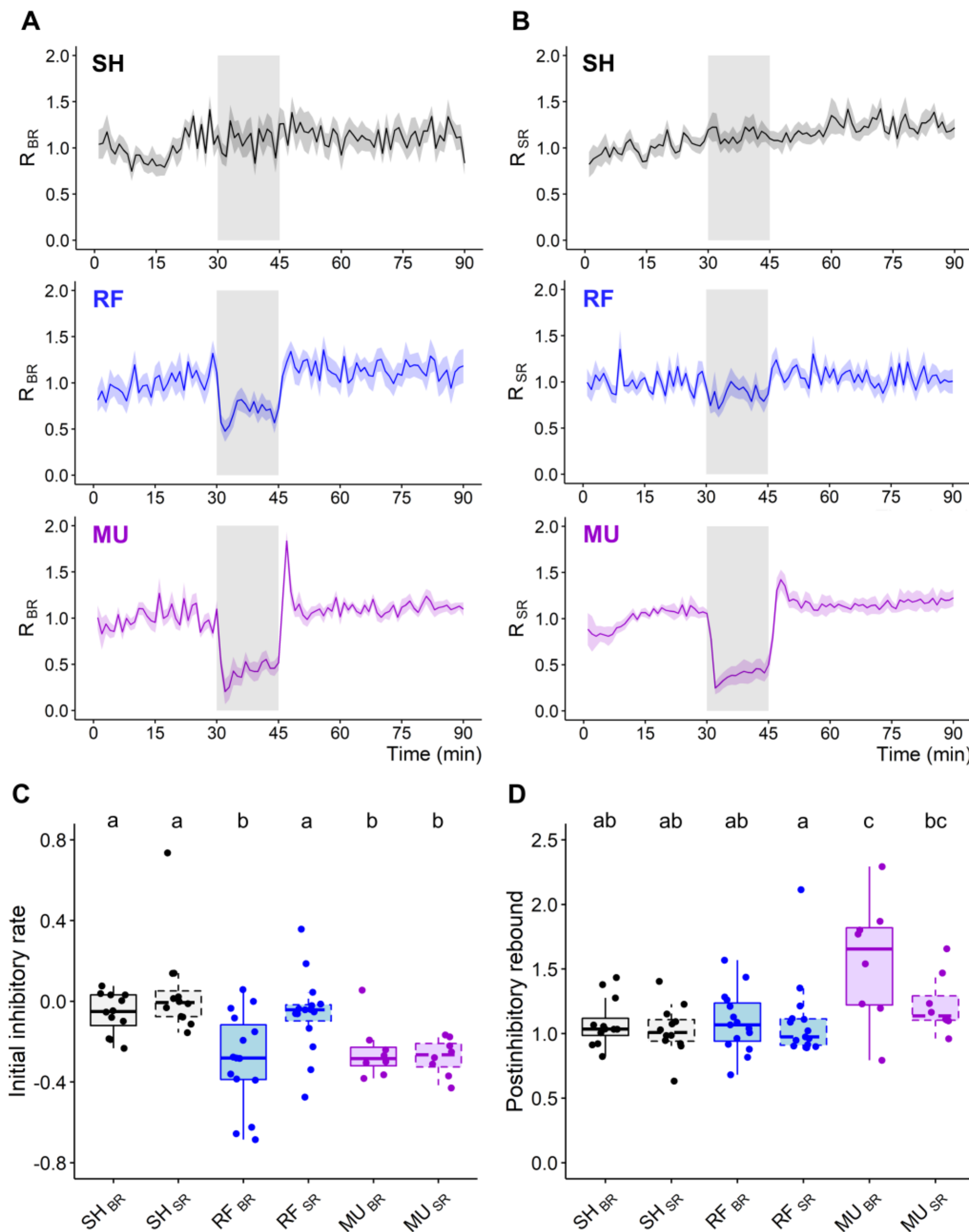

Fig 3. Temporal dynamic of RF and MU-induced inhibition on bursting and spiking rates. (A-B) Normalized temporal time course of bursting rate (BR, left) and spiking rate (SR, right) over 90 min for SH (top), RF (middle) and MU (bottom) groups (1 min bin-size, data show as Mean ± SEM). The exposure phase is symbolized by a gray shadowed area. **(C)** Initial inhibitory rate in response to RF and MU exposure. **(D)** Quantification of the postinhibitory rebound in response to treatment cessation. Boxplots with dashed box denote SR data. SH, n = 12; RF, n = 15; MU, n = 8. (C-D). Lower case letters indicate significant differences between groups.

319

320 Similarities and differences in the temporal domain between the two treatments are once again
321 exemplified in Figs 4A and 4B with data from two representative cultures exposed either to RF
322 fields or MU. In these examples, the MU experiment is initially marked by an abrupt shutdown

bioRxiv preprint doi: https://doi.org/10.1101/2022.04.05.487108; this version posted August 9, 2022. The copyright holder for this preprint (which was not certified by peer review) is the author/funder, who has granted bioRxiv a license to display the preprint in perpetuity. It is made available under aCC-BY-NC-ND 4.0 International license.

323 of neural activity, lasting a few minutes, followed by a slight and gradual return of activity.
324 Following washout of MU, network BR undergoes a short period of rebound excitation which
325 then re-stabilizes (note the absence of rebound excitation for SR). On the contrary, the RF ex-
326 posure experiment did not display such dynamics but was rather associated with a strict slow-
327 down of network activity with bursts peaking less frequently above the normalization line.

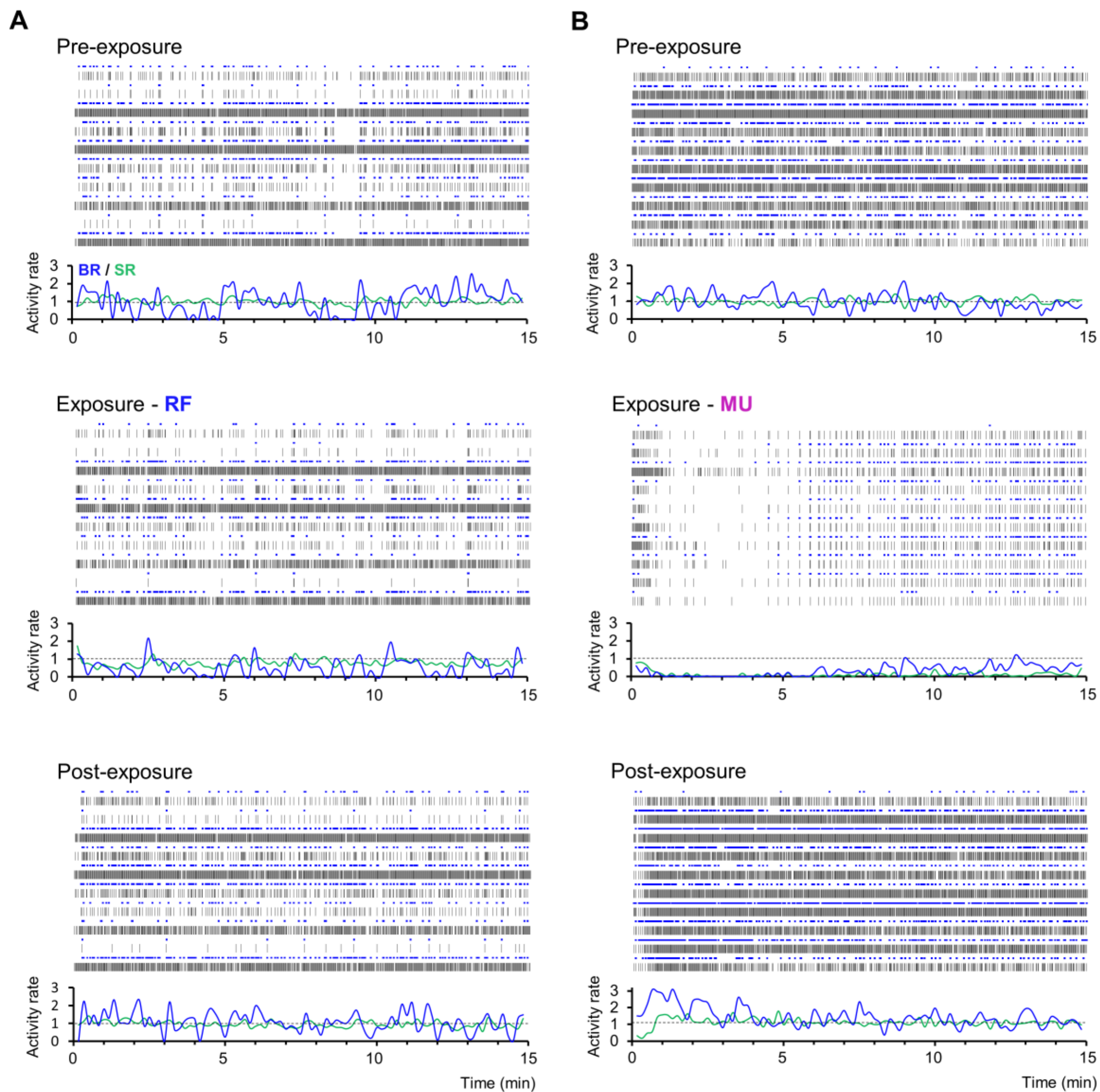

Fig 4. Representative recordings showing the temporal time course of RF- and MU-induced inhibition of neural networks. (A-B) Data from 10-selected electrodes of 2 independent cultures either exposed to RF (left) or MU (right) showing spiking (SR) and bursting rate (BR) along three recording segments of 15 min during pre-exposure (top), exposure (middle), and post-exposure recording phases (bottom). Neural activity is shown as spike raster plot capped in blue for markers of burst detection. Below each raster plot is the corresponding normalized BR (blue) and SR (green) computed overtime along non-overlapping sliding windows of 10 sec, dashed lines representing the normalization level.

328

bioRxiv preprint doi: https://doi.org/10.1101/2022.04.05.487108; this version posted August 9, 2022. The copyright holder for this preprint (which was not certified by peer review) is the author/funder, who has granted bioRxiv a license to display the preprint in perpetuity. It is made available under aCC-BY-NC-ND 4.0 International license.

329 ## RF and MU produce similar AP waveform alteration

330 The inhibitory effects of RF fields and MU were next analyzed and compared at the level of
331 single-unit activity by evaluating changes in AP waveforms (Fig 5). Definitions of the metrics
332 used to describe changes in AP waveform are illustrated in S1C Fig and defined in S3 Table.
333 To assess the magnitude of the reported normalized effects in respect to the raw data, raw data
334 at baseline relative to Fig 5 are tabulated in S4 Table. After hierarchical clustering of spike
335 events, data from the two main AP clusters were analyzed in a pooled manner (see materials
336 and methods section and S1 Fig for more details on AP detection, sorting, cluster repartition
337 and waveform analysis).

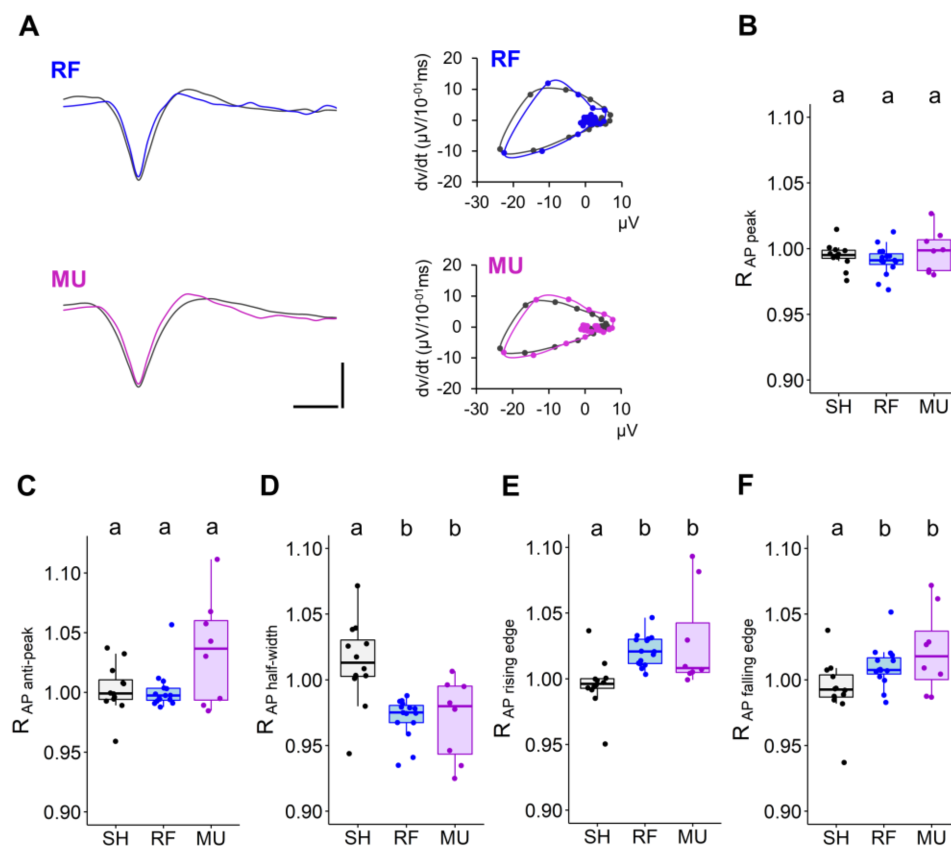

338 **Fig 5. Change in AP waveform in response to RF and MU exposure. (A)** Representative average AP traces from a single unit (left) and associated phase plot (right) before and during exposure to RF (top) and MU (bottom). Scale: (y): 15 µV; (x): 500 µs. **(B-F)** Boxplots showing variation in AP peak (B) and anti-peak amplitude (C) half-width (D) maximal rising (E) and falling edge (F). Normalized data, ratio of the exposure phase to baseline. SH, n = 12; RF, n = 15; MU, n = 8. (B-F). Lower case letters indicate significant differences between groups.

bioRxiv preprint doi: https://doi.org/10.1101/2022.04.05.487108; this version posted August 9, 2022. The copyright holder for this preprint (which was not certified by peer review) is the author/funder, who has granted bioRxiv a license to display the preprint in perpetuity. It is made available under aCC-BY-NC-ND 4.0 International license.

339 The average effects on AP waveform in response to RF fields and MU are shown from two
340 representative single units and their respective phase plots in Fig 5A. Analysis of AP waveforms
341 showed that, in respect to SH, RF and MU exposure neither impacted the AP peak amplitude
342 ($p = 0.3511$ - Fig 5B) nor the anti-peak amplitude ($p = 0.2859$ - Fig 5C), but that both treatments
343 narrowed the AP half-width (SH/RF, $p < 0.001$; SH/MU, $p = 0.0018$; RF/MU, $p = 0.6065$ - Fig
344 5D). This narrowing effect occurred symmetrically with both depolarization and repolarization
345 phases occurring at a faster rate (slope of the rising edge: SH/RF, $p < 0.001$; SH/MU, $p =$
346 0.0038; RF/MU, $p = 0.3547$ - Fig 5E; slope of the falling edge: SH/RF, $p = 0.0374$; SH/MU, p
347 $= 0.0224$; RF/MU, $p = 0.5659$ - Fig 5F). As confirmation, phase plots generally show steeper
348 slopes along the AP cycle, albeit of small amplitude. Analysis of the size effect indicated a
349 stronger effect on the rising than on the falling edge of the AP (RF: $\varepsilon^2_{rising} = 0.475$; $\varepsilon^2_{falling} =$
350 0.194; MU: $\varepsilon^2_{rising} = 0.384$; $\varepsilon^2_{falling} = 0.180$) suggesting that narrowing of the AP half-width in
351 response to RF and MU exposure occurred primarily through a mechanism that increases the
352 depolarization slope.
353

354

Discussion

355 In the present study, exposure to RF fields were performed at an SAR level of 28.6 W/kg, a
356 value ~1.4 times lower than levels used in [27-28]. Indeed, a recent re-evaluation of the dosim-
357 etry [42] indicated estimated SAR values per Watt of incident power of 5.5 ± 2.3 W/kg and
358 40.3 ± 5.3 W/kg respectively for the present and earlier MEA versions [27-28]. This re-evalu-
359 ation was made possible thanks to the continuous progress in experimental and numerical do-
360 simetry and better assessment of influencing environmental factors [42]. The SAR level of 28.6
361 W/kg is however higher than local basic safety restrictions fixed at 2.0 W/kg [13]. Therefore
362 this study is rather limited regarding the potential adverse effects of man-made environmental
363 RF fields on human health. RF exposure for 15 min at an SAR level of 28.6 W/kg decreased

bioRxiv preprint doi: https://doi.org/10.1101/2022.04.05.487108; this version posted August 9, 2022. The copyright holder for this preprint (which was not certified by peer review) is the author/funder, who has granted bioRxiv a license to display the preprint in perpetuity. It is made available under aCC-BY-NC-ND 4.0 International license.

364 reversibly bursting activity of ~35 % and co-occurred with an elevation of the culture medium
365 temperature of ~1 °C. The activity rate of neural culture is influenced by temperature with hypo-
366 and hyperthermia being respectively associated with lower and heightened neural activity [28,
367 36, 59-60] but see [61]. In line with data reported in these studies, previous experiments from
368 our lab showed that heating of the culture medium by ~1 °C slightly increased bursting activity
369 [28] thus suggesting that the observed effect of RF fields might have, in part, non-thermal ori-
370 gins.
371 We have previously reported that exposure to RF fields decreases the bursting activity of cul-
372 tured networks of cortical neurons [27] and that this inhibitory effect increases as exposure time
373 and SAR levels increase [28]. In the present study, investigations of the inhibitory effects of RF
374 fields were pursued by performing a direct comparison with the effects of the $GABA_A$ receptor
375 agonist MU. Our results showed that in contrast to MU, RF exposure preferentially inhibits
376 bursting over spiking activity. Although spiking activity was reduced by RF exposure, inhibi-
377 tion was more variable and weaker than for bursting activity. Other studies with cultured net-
378 works of cortical neurons also reported that MU equivalently inhibits spiking and bursting ac-
379 tivity [47, 57]. GABAergic inhibition in the brain can be classified as either phasic or tonic
380 [62]. The first depends on fast activation of synaptic $GABA_A$ receptors from synaptically re-
381 leased GABA, whereas the second depends on sustained activation of peri- and extrasynaptic
382 $GABA_A$ receptors by ambient GABA. In our experiments, continuous application of MU in the
383 culture medium activates both synaptic and peri-extrasynaptic $GABA_A$ receptors, which ulti-
384 mately leads to a tonic neural hyperpolarization. Neuronal excitability is in essence equivalently
385 reduced throughout the network subcomponents and an equivalent reduction in activity patterns
386 based on regular spiking, intrinsically bursting neurons as well on network collective bursting
387 behavior is observed. As RF exposure differentially impacted spiking and bursting activity, one
388 may argue that cell hyperpolarization is not the main force driving the inhibitory effects of RF

bioRxiv preprint doi: https://doi.org/10.1101/2022.04.05.487108; this version posted August 9, 2022. The copyright holder for this preprint (which was not certified by peer review) is the author/funder, who has granted bioRxiv a license to display the preprint in perpetuity. It is made available under aCC-BY-NC-ND 4.0 International license.

389 on neural networks. Studies on the effect of RF exposure on the membrane potential of excitable
390 cells (cardiomyocytes and neurons) has led to conflicting results, with some showing no effect
391 [23, 26, 63-64], others showing hyperpolarization [31], and sometimes both, depending on the
392 region studied after acute exposure of the whole animal [34]. Detailed electrophysiological in-
393 vestigations in our experimental conditions are needed to shed light on this point.
394 At the cellular level, cortical neurons can generate bursts based on intrinsic properties such as
395 hyperpolarization-activated current (I_h), subthreshold membrane oscillations and T-type cal-
396 cium current, above which high frequency action potentials fire for a brief period [65-67]. At a
397 network level, bursts can be generated intermittently in a collective manner as an emergent
398 property [68-69] relying on the development of an excitatory-inhibitory oscillating network
399 [70-71]. On that note, possible hypotheses could be that reduced bursting activity in response
400 to RF exposure is due to a predominant action on intrinsically bursting neurons over regular
401 spiking neurons or, alternatively, that the effect of RF manifests itself on a larger scale by re-
402 ducing network collective bursting behavior. Interestingly, some authors have suggested that
403 the extremely low-frequency EMFs (high-intensity power frequency, 50 Hz) enhance the ac-
404 tivity of cultured networks of cortical neurons by modulating the activity of pacemaker-like
405 interneurons [38]. To our knowledge, this research avenue has not yet been further investigated
406 by other laboratories. Nevertheless, our experiments focused on mature neocortical cultures
407 where network bursts substantially contribute to the overall burst count (~60 to ~80% of the
408 total number of bursts) and no discrimination in our analysis was considered between isolated
409 bursts and network bursts. Therefore, the observed inhibition of bursting activity in response to
410 RF exposure mostly originates from a reduction of network collective bursting behavior. RF
411 exposure at different levels of culture maturity (i.e. irregular and slightly synchronized bursting
412 vs. regular and highly synchronized bursting) is of interest to determine whether neural network
413 topology is a factor determining the sensitivity to RF fields. Moreover, detailed analysis with

bioRxiv preprint doi: https://doi.org/10.1101/2022.04.05.487108; this version posted August 9, 2022. The copyright holder for this preprint (which was not certified by peer review) is the author/funder, who has granted bioRxiv a license to display the preprint in perpetuity. It is made available under aCC-BY-NC-ND 4.0 International license.

414 improved detection algorithms could help to better differentiate between the effect of RF expo-
415 sure on the different network subcomponents and related activity patterns.
416 Descriptors of neural networks bursting activity were similarly impacted by RF and MU expo-
417 sure. In the two forms of inhibition, decreased MBR was accompanied by increased IBI and
418 decreased BD, but data suggested that only inhibition induced by MU was accompanied by
419 increased IBSR. However, the reported effect of MU on IBSR seems to contradict the results
420 of a recent thorough study done under similar experimental conditions [47], thus making it
421 difficult to evaluate the pertinence of this observation in comparison to RF exposure. At neural
422 networks level, a shift in the balance between excitation and inhibition strongly contributes to
423 control burst phase, termination and intraburst spiking rate [47-48, 72-73]. Both Inhibition and
424 disinhibition cause a shortening of the BD . The former occurs with reduced IBSR whereas the
425 second occurs with increased IBSR. Indicators of network bursting synchronization were dif-
426 ferently impacted by RF and MU exposure. During the two forms of inhibition BD and IBSR
427 synchronization decreased over the network but only MU shifted network bursting behavior
428 from regular and synchronized to more irregular and less synchronized. This observation sug-
429 gests that the effects of RF exposure exert fewer constraints on network functioning than those
430 mediated by the activation of the $GABA_A$ receptor. The desynchronizing effect of MU on net-
431 work bursting behavior can most likely be attributed to its hyperpolarizing action. Indeed, it has
432 been shown that inverting the polarity of the GABA action, i.e. depolarizing toward hyperpo-
433 larizing, can evoke desynchronized premature-like network activity in young, moderately syn-
434 chronized, cultures [48].
435 Upon recovery from the inhibitory effects of MU but not from those of RF exposure, networks
436 showed a dramatic regain in bursting activity that persisted recurrently in a synchronous manner
437 for ~1 min. This phenomenon relies most likely on the intrinsic property of cortical neurons’

bioRxiv preprint doi: https://doi.org/10.1101/2022.04.05.487108; this version posted August 9, 2022. The copyright holder for this preprint (which was not certified by peer review) is the author/funder, who has granted bioRxiv a license to display the preprint in perpetuity. It is made available under aCC-BY-NC-ND 4.0 International license.

438 so-called postinhibitory rebound and refers to the ability of a neuron to generate rebound exci-
439 tation upon termination of an inhibitory signal [74-75]. Postinhibitory rebound is involved in a
440 variety of basic brain processes such as rhythmic recurrent activity [76] and short-term plastic-
441 ity [77]. This phenomenon relies on several mechanisms occurring in response to hyperpolari-
442 zation such as activation of hyperpolarization-activated cyclic nucleotide-gated (HCN) chan-
443 nels and deinactivation of low voltage-activated T-type calcium channels and persistent sodium
444 channels [78-81]. In our conditions, postinhibitory rebound occurred in response to washout of
445 MU and consecutive removal of tonic hyperpolarization. The absence of postinhibitory rebound
446 in response to RF exposure cessation might furthermore imply that RF fields exert their inhib-
447 itory effects without hyperpolarizing neurons. Reduced bursting activity combined with the
448 lack of postinhibitory rebound might suggest that RF fields potentially interfere with the func-
449 tioning of ion channels involved in these modalities such as of HCN, T-type calcium channels
450 and persistent sodium channels. Interestingly, it has been reported that exposure to extremely
451 low-frequency-EMF (50 Hz, 0.2 mT, 1 hour) inhibited T-type calcium channels in mouse cor-
452 tical neurons [82]. However, no comparison with other types of currents was made, making it
453 difficult to assess the relevance of this observation in the present study (see [83-84] for reviews
454 on EMF and calcium). Nevertheless, the rapid onset of the effects of RF fields and their revers-
455 ibility are in favor of a mechanism interacting with fast operating targets at the membrane level
456 such as ion channels. For a detailed review on EMF with cell membranes, organelles and bio-
457 molecules see [19]. Thorough investigations with co-exposure of RF fields and pharmacologi-
458 cal agents will enable directly testing potential interactions with ion channels.

459 Analysis of AP waveform showed that RF- and MU-induced inhibition co-occurred with a
460 slight symmetrical narrowing effect of the AP half-width. Although other studies have reported
461 on the narrowing effect of RF exposure on AP waveform [29, 31, 34] (but see [26, 30]), the
462 mechanism of action through which RF fields alter the AP waveform remains to be established.

bioRxiv preprint doi: https://doi.org/10.1101/2022.04.05.487108; this version posted August 9, 2022. The copyright holder for this preprint (which was not certified by peer review) is the author/funder, who has granted bioRxiv a license to display the preprint in perpetuity. It is made available under aCC-BY-NC-ND 4.0 International license.

463 Changes in the AP half-width exert direct influences on the efficacy of synaptic transmission
464 [85-88] and might contribute to the inhibitory effect of RF exposure on network bursting activ-
465 ity. Commonalities in the changes in AP waveforms in response to RF and MU exposure sug-
466 gest a potential overlapping mechanism between these two modalities. A possible point of con-
467 vergence could be a similar effect on the membrane resistance. Indeed, a decrease in membrane
468 resistance in response to MU [89-90] has also been observed in response to RF fields [22-23]
469 but see [25-26, 91] and millimeter waves (MMWs, 30-300 GHz) [29]. The AP shape strongly
470 relates to membrane resistance, with decreased and increased resistance being respectively as-
471 sociated with narrower and broader AP [92-93]. Membrane resistance and AP waveform are
472 also very sensitive to changes in temperature with increased and decreased temperature leading
473 respectively to lower/narrower and higher/broader membrane resistance and AP [92-95]. There-
474 fore, it cannot be excluded that the observed effect on AP waveform has a thermal origin [31].
475 Recently, it has been reported that mid-infrared radiations also shorten AP by accelerating its
476 repolarization, through an increase in voltage-gated potassium currents [95]. Mechanisms of
477 RF field effects might differ from mid-infrared radiation as they manifest predominantly by a
478 steeper depolarization phase. Detailed electrophysiological experiments combined with accu-
479 rate temperature control or bulk heating are required to elucidate the mechanism of RF fields
480 on AP waveform. Moreover, the hypothesis that decreased AP half-width contributes to de-
481 creased network bursting behavior should be investigated in silico with neural simulation.
482

483 ## Acknowledgments

484 The authors thank Stephano Buccelli for his contribution in implementing new scripts in the
485 software package SPYCODE and Prof. Dr. Patrik Krieger for sharing tools for spike sorting.

486

bioRxiv preprint doi: https://doi.org/10.1101/2022.04.05.487108; this version posted August 9, 2022. The copyright holder for this preprint (which was not certified by peer review) is the author/funder, who has granted bioRxiv a license to display the preprint in perpetuity. It is made available under aCC-BY-NC-ND 4.0 International license.

487 # Author Contributions

488 **Conceptualization:** André Garenne, Isabelle Lagroye, Noëlle Lewis.

489 **Data Curation:** Clément E. Lemercier.

490 **Formal Analysis:** Clément E. Lemercier.

491 **Funding Acquisition:** André Garenne, Delia Arnaud-Cormos, Philippe Levêque, Isabelle La-
492 groye, Noëlle Lewis.

493 **Investigation :** Clément E. Lemercier.

494 **Methodology:** Clément E. Lemercier, André Garenne, Florence Poulletier de Gannes, Corinne
495 El Khoueiry, Delia Arnaud-Cormos, Philippe Levêque, Isabelle Lagroye, Yann Percherancier,
496 Noëlle Lewis.

497 **Project Administration:** Noëlle Lewis.

498 **Resources:** Noëlle Lewis.

499 **Supervision:** André Garenne, Noëlle Lewis.

500 **Visualization:** Clément E. Lemercier.

501 **Writing – Original Draft Preparation:** Clément E. Lemercier

502 **Writing – Review & Editing:** Clément E. Lemercier, André Garenne, Florence Poulletier de
503 Gannes, Corinne El Khoueiry, Delia Arnaud-Cormos, Philippe Levêque, Isabelle Lagroye,
504 Yann Percherancier, Noëlle Lewis.

505

506 # Data Availability Statement

507 All relevant data are within the manuscript and its Supporting Information files.

508

509 # Funding

510 This work was supported by the French National Research Program for Environmental and
511 Occupational Health of ANSES under Grant 2015/2 RF/19, by the European Union's Horizon
512 2020 Research and Innovation Program under Grant 737164 and by the Region Nouvelle-Aq-
513 uitaine under Grant AAPR2020A-2019-8152210. The funders had no role in study design, data
514 collection and analysis, decision to publish, or preparation of the manuscript.

bioRxiv preprint doi: https://doi.org/10.1101/2022.04.05.487108; this version posted August 9, 2022. The copyright holder for this preprint (which was not certified by peer review) is the author/funder, who has granted bioRxiv a license to display the preprint in perpetuity. It is made available under aCC-BY-NC-ND 4.0 International license.

515

516 # Competing interests

517 The authors have declared that no competing interests exist.

518

519 # References

520 1. van Rongen E, Croft R, Juutilainen J, Lagroye I, Miyakoshi J, Saunders R, et al. Effects of
521 Radiofrequency Electromagnetic Fields on the Human Nervous System. Journal of Toxi-
522 cology and Environmental Health, Part B. 2009;12: 572–597.
523 https://doi.org/10.1080/10937400903458940 PMID: 20183535

524 2. Hossmann K-A, Hermann DM. Effects of electromagnetic radiation of mobile phones on
525 the central nervous system. Bioelectromagnetics. 2003;24: 49–62.
526 https://doi.org/10.1002/bem.10068 PMID: 12483665

527 3. Kim JH, Lee J-K, Kim H-G, Kim K-B, Kim HR. Possible Effects of Radiofrequency Elec-
528 tromagnetic Field Exposure on Central Nerve System. Biomolecules & Therapeutics.
529 2019;27: 265–275. https://doi.org/10.4062/biomolther.2018.152 PMID: 30481957

530 4. Croft RJ, Hamblin DL, Spong J, Wood AW, McKenzie RJ, Stough C. The effect of mobile
531 phone electromagnetic fields on the alpha rhythm of human electroencephalogram. Bioe-
532 lectromagnetics. 2008;29: 1–10. https://doi.org/10.1002/bem.20352 PMID: 17786925

533 5. Croft RJ, Leung S, McKenzie RJ, Loughran SP, Iskra S, Hamblin DL, Cooper NR. Effects
534 of 2G and 3G mobile phones on human alpha rhythms: Resting EEG in adolescents, young
535 adults, and the elderly. Bioelectromagnetics. 2010 Sep;31(6):434-44.
536 https://doi.org/10.1002/bem.20583 PMID: 20564174

537 6. Schmid MR, Loughran SP, Regel SJ, Murbach M, Bratic Grunauer A, Rusterholz T, et al.
538 Sleep EEG alterations: effects of different pulse-modulated radio frequency electromag-
539 netic fields: Different pulse-modulated RF EMF and sleep EEG. Journal of Sleep Research.
540 2012;21: 50–58. https://doi.org/10.1111/j.1365-2869.2011.00918.x PMID: 21489004

541 7. Wallace J, Yahia-Cherif L, Gitton C, Hugueville L, Lemaréchal JD, Selmaoui B. Modula-
542 tion of magnetoencephalography alpha band activity by radiofrequency electromagnetic
543 field depicted in sensor and source space. Sci Rep. déc 2021;11(1):23403.
544 https://doi.org/10.1038/s41598-021-02560-0 PMID: 34862418

545 8. Wallace J, Selmaoui B. Effect of mobile phone radiofrequency signal on the alpha rhythm
546 of human waking EEG: A review. Environ Res. 2019 Aug;175:274-286.
547 https://doi.org/10.1016/j.envres.2019.05.016 PMID: 31146099

bioRxiv preprint doi: https://doi.org/10.1101/2022.04.05.487108; this version posted August 9, 2022. The copyright holder for this preprint (which was not certified by peer review) is the author/funder, who has granted bioRxiv a license to display the preprint in perpetuity. It is made available under aCC-BY-NC-ND 4.0 International license.

548 9. Eulitz C, Ullsperger P, Freude G, Elbert T. Mobile phones modulate response patterns of
549 human brain activity. NeuroReport. 1998;9: 3229–3232. https://doi.org/10.1097/00001756-
550 199810050-00018 PMID: 9831456

551 10. Ferreri F, Curcio G, Pasqualetti P, De Gennaro L, Fini R, Rossini PM. Mobile phone emis-
552 sions and human brain excitability. Ann Neurol. 2006;60: 188–196.
553 https://doi.org/10.1002/ana.20906 PMID: 16802289

554 11. Kleinlogel H, Dierks Th, Koenig Th, Lehmann H, Minder A, Berz R. Effects of weak mo-
555 bile phone-Electromagnetic fields (GSM, UMTS) on event related potentials and cognitive
556 functions. Bioelectromagnetics. 2008;29: 488–497. https://doi.org/10.1002/bem.20418
557 PMID: 18421712

558 12. Volkow ND, Tomasi D, Wang GJ, Vaska P, Fowler JS, Telang F, Alexoff D, Logan J,
559 Wong C. Effects of cell phone radiofrequency signal exposure on brain glucose metabolism.
560 JAMA. 2011 Feb 23;305(8):808-13. https://doi.org/10.1001/jama.2011.186 PMID:
561 21343580

562 13. ICNIRP (International Commission on Non-Ionizing Radiation Protection). Guidelines for
563 Limiting Exposure to Electromagnetic Fields (100 kHz to 300 GHz). Health Phys. 2020
564 May;118(5):483-524. https://doi.org/10.1097/HP.0000000000001210 PMID: 32167495

565 14. SCENIHR (Scientific Committee on Emerging and Newly Identified Health Risks). Poten-
566 tial health effects of exposure to electromagnetic fields (EMF). European Commission
567 2015: 1–288, 2015. https://doi.org/10.2772/75635

568 15. Foster KR, Glaser R. Thermal mechanisms of interaction of radiofrequency energy with
569 biological systems with relevance to exposure guidelines. Health Physics. 2007;92: 609–
570 620. https://doi.org/10.1097/01.HP.0000262572.64418.38 PMID: 17495663

571 16. Greenebaum B, Barnes F. Handbook of Biological Effects of Electromagnetic Fields, Vol.
572 1. Biological and Medical Aspects of Electromagnetic Fields 4th edn. (CRC Press, Boca
573 Raton, 2019).

574 17. Belpomme D, Hardell L, Belyaev I, Burgio E, Carpenter DO. Thermal and non-thermal
575 health effects of low intensity non-ionizing radiation: An international perspective. Envi-
576 ronmental Pollution. 2018;242: 643–658. https://doi.org/10.1016/j.envpol.2018.07.019
577 PMID: 30025338

578 18. Hinrikus H, Bachmann M, Lass J. Understanding physical mechanism of low-level micro-
579 wave radiation effect. International Journal of Radiation Biology. 2018;94: 877–882.
580 https://doi.org/10.1080/09553002.2018.1478158 PMID: 29775391

581 19. Romanenko S, Begley R, Harvey AR, Hool L, Wallace VP. The interaction between elec-
582 tromagnetic fields at megahertz, gigahertz and terahertz frequencies with cells, tissues and
583 organisms: risks and potential. J R Soc Interface. 2017;14: 20170585.
584 https://doi.org/10.1098/rsif.2017.0585 PMID: 29212756

bioRxiv preprint doi: https://doi.org/10.1101/2022.04.05.487108; this version posted August 9, 2022. The copyright holder for this preprint (which was not certified by peer review) is the author/funder, who has granted bioRxiv a license to display the preprint in perpetuity. It is made available under aCC-BY-NC-ND 4.0 International license.

585 20. Apollonio F, Liberti M, Paffi A, Merla C, Marracino P, Denzi A, et al. Feasibility for Mi-
586 crowaves Energy to Affect Biological Systems Via Nonthermal Mechanisms: A Systematic
587 Approach. IEEE Trans Microwave Theory Techn. 2013;61: 2031–2045.
588 https://doi.org/10.1109/TMTT.2013.2250298

589 21. Foster KR. Thermal and nonthermal mechanisms of interaction of radio-frequency energy
590 with biological systems. IEEE Trans Plasma Sci. 2000;28: 15–23.
591 https://doi.org/10.1109/27.842819

592 22. Arber SL. The Effect of Microwave Radiation on Passive Membrane Properties of Snail
593 Neurons. Journal of Microwave Power. 1981;16: 15–20.
594 https://doi.org/10.1080/16070658.1981.11689217 PMID: 6787208

595 23. Arber SL, Lin JC. Microwave-induced changes in nerve cells: Effects of modulation and
596 temperature. Bioelectromagnetics. 1985;6: 257–270.
597 https://doi.org/10.1002/bem.2250060306 PMID: 3836669

598 24. Bolshakov MA, Alekseev SI. Bursting responses of Lymnea neurons to microwave radia-
599 tion. Bioelectromagnetics. 1992;13: 119–129. https://doi.org/10.1002/bem.2250130206
600 PMID: 1590812

601 25. Ginsburg KS, Lin JC, O'Neill WD. Microwave effects on input resistance and action po-
602 tential firing of snail neurons. IEEE Trans Biomed Eng. 1992;39: 1011–1021.
603 https://doi.org/10.1109/10.161333 PMID: 1280617

604 26. Wachtel H, Seaman R, Joines W. Effects of low-intensity microwaves on isolated neurons.
605 Ann NY Acad Sci. 1975;247: 46–62. https://doi.org/10.1111/j.1749-6632.1975.tb35982.x
606 PMID: 1054247

607 27. Moretti D, Garenne A, Haro E, Poulletier de Gannes F, Lagroye I, Lévêque P, et al. In-vitro
608 exposure of neuronal networks to the GSM-1800 signal: GSM-1800 Exposure of Neuronal
609 Networks. Bioelectromagnetics. 2013;34: 571–578. https://doi.org/10.1002/bem.21805
610 PMID: 23913345

611 28. El Khoueiry C, Moretti D, Renom R, Camera F, Orlacchio R, Garenne A, et al. Decreased
612 spontaneous electrical activity in neuronal networks exposed to radiofrequency 1,800 MHz
613 signals. Journal of Neurophysiology. 2018;120: 2719–2729.
614 https://doi.org/10.1152/jn.00589.2017 PMID: 30133383

615 29. Pikov V, Arakaki X, Harrington M, Fraser SE, Siegel PH. Modulation of neuronal activity
616 and plasma membrane properties with low-power millimeter waves in organotypic cortical
617 slices. J Neural Eng. 2010;7: 045003. https://doi.org/10.1088/1741- 2560/7/4/045003
618 PMID: 20644247

619 30. Razavinasab M, Moazzami K, Shabani M. Maternal mobile phone exposure alters intrinsic
620 electrophysiological properties of CA1 pyramidal neurons in rat offspring. Toxicol Ind
621 Health. 2016;32: 968–979. https://doi.org/10.1177/0748233714525497 PMID: 24604340

bioRxiv preprint doi: https://doi.org/10.1101/2022.04.05.487108; this version posted August 9, 2022. The copyright holder for this preprint (which was not certified by peer review) is the author/funder, who has granted bioRxiv a license to display the preprint in perpetuity. It is made available under aCC-BY-NC-ND 4.0 International license.

622 31. Romanenko S, Siegel PH, Wagenaar DA, Pikov V. Effects of millimeter wave irradiation
623 and equivalent thermal heating on the activity of individual neurons in the leech ganglion.
624 Journal of Neurophysiology. 2014;112: 2423–2431. https://doi.org/10.1152/jn.00357.2014
625 PMID: 25122711

626 32. Saito A, Takahashi M, Jimbo Y, Nakasono S. Non-conductive and miniature fiber-optic
627 imaging system for real-time detection of neuronal activity in time-varying electromagnetic
628 fields. Biosensors and Bioelectronics. 2017;87: 786–793.
629 https://doi.org/10.1016/j.bios.2016.09.024 PMID: 27649336

630 33. Tattersall JEH, Scott IR, Wood SJ, Nettell JJ, Bevir MK, Wang Z, et al. Effects of low
631 intensity radiofrequency electromagnetic fields on electrical activity in rat hippocampal
632 slices. Brain Research. 2001;904: 43–53. https://doi.org/10.1016/S0006-8993(01)02434-9
633 PMID: 11516410

634 34. Wang K, Lu J-M, Xing Z-H, Zhao Q-R, Hu L-Q, Xue L, et al. Effect of 1.8 GHz radiofre-
635 quency electromagnetic radiation on novel object associative recognition memory in mice.
636 Sci Rep. 2017;7: 44521. https://doi.org/10.1038/srep44521 PMID: 28303965

637 35. Xu S, Ning W, Xu Z, Zhou S, Chiang H, Luo J. Chronic exposure to GSM 1800-MHz
638 microwaves reduces excitatory synaptic activity in cultured hippocampal neurons. Neuro-
639 science Letters. 2006;398: 253–257. https://doi.org/10.1016/j.neulet.2006.01.004 PMID:
640 16443327

641 36. Köhler T, Wölfel M, Ciba M, Bochtler U, Thielemann C. Terrestrial Trunked Radio
642 (TETRA) exposure of neuronal in vitro networks. Environmental Research. 2018;162: 1–
643 7. https://doi.org/10.1016/j.envres.2017.12.007 PMID: 29272813

644 37. Oster S, Daus AW, Erbes C, Goldhammer M, Bochtler U, Thielemann C. Long-term elec-
645 tromagnetic exposure of developing neuronal networks: A flexible experimental setup: Ex-
646 posure of Developing Neuronal Networks. Bioelectromagnetics. 2016;37: 264–278.
647 https://doi.org/10.1002/bem.21974 PMID: 27070808

648 38. Saito A, Takahashi M, Makino K, Suzuki Y, Jimbo Y, Nakasono S. Response of Cultured
649 Neuronal Network Activity After High-Intensity Power Frequency Magnetic Field Expo-
650 sure. Front Physiol. 2018;9: 189. https://doi.org/10.3389/fphys.2018.00189 PMID:
651 29662453

652 39. Merla C, Ticaud N, Arnaud-Cormos D, Veyret B, Leveque P. Real-Time RF Exposure
653 Setup Based on a Multiple Electrode Array (MEA) for Electrophysiological Recording of
654 Neuronal Networks. IEEE Trans Microwave Theory Techn. 2011;59: 755–762.
655 https://doi.org/10.1109/TMTT.2010.2100404

656 40. Olsen RW, Sieghart W. International Union of Pharmacology. LXX. Subtypes of γ-Ami-
657 nobutyric Acid A Receptors: Classification on the Basis of Subunit Composition, Pharma-
658 cology, and Function. Update. Pharmacol Rev. 2008;60: 243–260.
659 https://doi.org/10.1124/pr.108.00505 PMID: 18790874

bioRxiv preprint doi: https://doi.org/10.1101/2022.04.05.487108; this version posted August 9, 2022. The copyright holder for this preprint (which was not certified by peer review) is the author/funder, who has granted bioRxiv a license to display the preprint in perpetuity. It is made available under aCC-BY-NC-ND 4.0 International license.

660 41. Sallard E, Letourneur D, Legendre P. Electrophysiology of ionotropic GABA receptors.
661 Cell Mol Life Sci. 2021;78: 5341–5370. https://doi.org/10.1007/s00018-021-03846-2
662 PMID: 34061215

663 42. Nefzi A, Orlacchio R, Carr L, Lemercier CE, Khoueiry CE, Lewis N, et al. Dosimetry of
664 Microelectrodes Array Chips for Electrophysiological Studies Under Simultaneous Radio
665 Frequency Exposures. IEEE Trans Microwave Theory Techn. 2022;70: 1871–1881.
666 https://doi.org/10.1109/TMTT.2021.3136296

667 43. Soueid M, Kohler S, Carr L, Bardet SM, O'Connor RP, Leveque P, et al. Electromagnetic
668 Analysis of an Aperture Modified TEM Cell Including an ITO Layer for Real-Time Obser-
669 vation of Biological Cells Exposed to Microwaves. PIER. 2014;149: 193–204.
670 https://doi.org/10.2528/PIER14053108

671 44. Bologna LL, Pasquale V, Garofalo M, Gandolfo M, Baljon PL, Maccione A, et al. Investi-
672 gating neuronal activity by SPYCODE multi-channel data analyzer. Neural Networks.
673 2010;23: 685–697. https://doi.org/10.1016/j.neunet.2010.05.002 PMID: 20554151

674 45. Maccione A, Gandolfo M, Massobrio P, Novellino A, Martinoia S, Chiappalone M. A novel
675 algorithm for precise identification of spikes in extracellularly recorded neuronal signals.
676 Journal of Neuroscience Methods. 2009;177: 241–249.
677 https://doi.org/10.1016/j.jneumeth.2008.09.026 PMID: 18957306

678 46. Pasquale V, Martinoia S, Chiappalone M. A self-adapting approach for the detection of
679 bursts and network bursts in neuronal cultures. J Comput Neurosci. 2010;29: 213–229.
680 https://doi.org/10.1007/s10827-009-0175-1 PMID: 19669401

681 47. Bader BM, Steder A, Klein AB, Frølund B, Schroeder OHU, Jensen AA. Functional char-
682 acterization of GABAA receptor-mediated modulation of cortical neuron network activity
683 in microelectrode array recordings. Cymbalyuk G, editor. PLoS ONE. 2017;12: e0186147.
684 https://doi.org/10.1371/journal.pone.0186147 PMID: 29028808

685 48. Baltz T, de Lima AD, Voigt T. Contribution of GABAergic interneurons to the development
686 of spontaneous activity patterns in cultured neocortical networks. Front Cell Neurosci. 2010
687 Jun 21;4:15. https://doi.org/10.3389/fncel.2010.00015 PMID: 20617185

688 49. R Core Team. R: A language and environment for statistical computing. Vienna, Austria:
689 R Foundation for Statistical Computing, 2020. https://www.R-project.org/.
690

691 50. Pohlert T (2020). PMCMRplus: Calculate Pairwise Multiple Comparisons of Mean Rank
692 Sums Extended. R package version 1.4.4. https://CRAN.R-project.org/package=PMCMR-
693 plus

694 51. Mangiafico S. (2020). rcompanion: Functions to Support Extension Education Program
695 Evaluation. R package version 2.3.25. https://CRAN.R-project.org/package=rcompanion

696 52. Wickham H (2016). ggplot2: Elegant Graphics for Data Analysis. Springer-Verlag New
697 York. ISBN 978-3-319-24277-4, https://ggplot2.tidyverse.org

bioRxiv preprint doi: https://doi.org/10.1101/2022.04.05.487108; this version posted August 9, 2022. The copyright holder for this preprint (which was not certified by peer review) is the author/funder, who has granted bioRxiv a license to display the preprint in perpetuity. It is made available under aCC-BY-NC-ND 4.0 International license.

698 53. Kassambara A (2020). ggpubr: 'ggplot2' Based Publication Ready Plots. R package version
699 0.4.0. https://CRAN.R-project.org/package=ggpubr

700 54. Piepho H-P. An Algorithm for a Letter-Based Representation of All-Pairwise Comparisons.
701 Journal of Computational and Graphical Statistics. 2004;13: 456–466.
702 https://doi.org/10.1198/1061860043515

703 55. Graves S, Piepho H-P, and Selzer L with help from Dorai-Raj S (2019). multcompView:
704 Visualizations of Paired Comparisons. R package version 0.1-8. https://CRAN.R-pro-
705 ject.org/package=multcompView

706 56. Dunn SM, Thuynsma RP. Reconstitution of purified GABAA receptors: ligand binding and
707 chloride transporting properties. Biochemistry. 1994 Jan 25;33(3):755-63. https://doi.org/
708 10.1021/bi00169a017 PMID: 8292603

709 57. Novellino A, Scelfo B, Palosaari T, Price A, Sobanski T, Shafer TJ, et al. Development of
710 Micro-Electrode Array Based Tests for Neurotoxicity: Assessment of Interlaboratory Re-
711 producibility with Neuroactive Chemicals. Front Neuroeng. 2011;4.
712 https://doi.org/10.3389/fneng.2011.00004 PMID: 21562604

713 58. Rijal SO, Gross GW. Dissociation constants for GABAA receptor antagonists determined
714 with neuronal networks on microelectrode arrays. Journal of Neuroscience Methods.
715 2008;173: 183–192. https://doi.org/10.1016/j.jneumeth.2008.05.025 PMID: 18590768

716 59. Rubinsky L, Raichman N, Baruchi I, Shein M, Lavee J, Frenk H, et al. Study of hypothermia
717 on cultured neuronal networks using multi-electrode arrays. Journal of Neuroscience Meth-
718 ods. 2007;160: 288–293. https://doi.org/10.1016/j.jneumeth.2006.09.017 PMID: 17081617

719 60. Wang Y-Y, Qin J, Han Y, Cai J, Xing G-G. Hyperthermia induces epileptiform discharges
720 in cultured rat cortical neurons. Brain Research. 2011;1417: 87–102.
721 https://doi.org/10.1016/j.brainres.2011.08.027 PMID: 21907327

722 61. Zwartsen A, Hondebrink L, de Lange DW, Westerink RHS. Hyperthermia exacerbates the
723 acute effects of psychoactive substances on neuronal activity measured using microelec-
724 trode arrays (MEAs) in rat primary cortical cultures in vitro. Toxicology and Applied Phar-
725 macology. 2020;397: 115015. https://doi.org/10.1016/j.taap.2020.115015 PMID:
726 32320794

727 62. Farrant M, Nusser Z. Variations on an inhibitory theme: phasic and tonic activation of
728 GABAA receptors. Nat Rev Neurosci. 2005;6: 215–229. https://doi.org/10.1038/nrn1625
729 PMID: 15738957

730 63. Linz KW, von Westphalen C, Streckert J, Hansen V, Meyer R. Membrane potential and
731 currents of isolated heart muscle cells exposed to pulsed radio frequency fields. Bioelectro-
732 magnetics. 1999 Dec;20(8):497-511.https://doi.org/10.1002/(SICI)1521-
733 186X(199912)20:8<497::AID-BEM4>3.0.CO;2-5 PMID: 10559771

734 64. Marchionni I, Paffi A, Pellegrino M, Liberti M, Apollonio F, Abeti R, et al. Comparison
735 between low-level 50 Hz and 900 MHz electromagnetic stimulation on single channel ionic

bioRxiv preprint doi: https://doi.org/10.1101/2022.04.05.487108; this version posted August 9, 2022. The copyright holder for this preprint (which was not certified by peer review) is the author/funder, who has granted bioRxiv a license to display the preprint in perpetuity. It is made available under aCC-BY-NC-ND 4.0 International license.

736 currents and on firing frequency in dorsal root ganglion isolated neurons. Biochimica et
737 Biophysica Acta (BBA) - Biomembranes. 2006;1758: 597–605.
738 https://doi.org/10.1016/j.bbamem.2006.03.014 PMID: 16713990

739 65. Cain SM, Snutch TP. T-type calcium channels in burst-firing, network synchrony, and epi-
740 lepsy. Biochimica et Biophysica Acta (BBA) - Biomembranes. 2013;1828: 1572–1578.
741 https://doi.org/10.1016/j.bbamem.2012.07.028 PMID: 22885138

742 66. Perez-Reyes E. Molecular Physiology of Low-Voltage-Activated T-type Calcium Chan-
743 nels. Physiological Reviews. 2003;83: 117–161.
744 https://doi.org/10.1152/physrev.00018.2002 PMID: 12506128

745 67. Wu N, Hsiao C-F, Chandler SH. Membrane Resonance and Subthreshold Membrane Os-
746 cillations in Mesencephalic V Neurons: Participants in Burst Generation. J Neurosci.
747 2001;21: 3729–3739. https://doi.org/10.1523/JNEUROSCI.21-11-03729.2001 PMID:
748 11356860

749 68. van Pelt J, Wolters PS, Corner MA, Rutten WLC, Ramakers GJA. Long-Term Characteri-
750 zation of Firing Dynamics of Spontaneous Bursts in Cultured Neural Networks. IEEE Trans
751 Biomed Eng. 2004;51: 2051–2062. https://doi.org/10.1109/TBME.2004.827936 PMID:
752 15536907

753 69. Wagenaar D, Pine J, Potter S. An extremely rich repertoire of bursting patterns during the
754 development of cortical cultures. BMC Neurosci. 2006;7: 11. https://doi.org/10.1186/1471-
755 2202-7-11 PMID: 16464257

756 70. Fardet T, Ballandras M, Bottani S, Métens S, Monceau P. Understanding the Generation of
757 Network Bursts by Adaptive Oscillatory Neurons. Front Neurosci. 2018;12: 41.
758 https://doi.org/10.3389/fnins.2018.00041 PMID: 29467607

759 71. Teppola H, Aćimović J, Linne M-L. Unique Features of Network Bursts Emerge From the
760 Complex Interplay of Excitatory and Inhibitory Receptors in Rat Neocortical Networks.
761 Front Cell Neurosci. 2019;13: 377. https://doi.org/10.3389/fncel.2019.00377 PMID:
762 31555093

763 72. Arnold FJL, Hofmann F, Bengtson CP, Wittmann M, Vanhoutte P, Bading H. Microelec-
764 trode array recordings of cultured hippocampal networks reveal a simple model for tran-
765 scription and protein synthesis-dependent plasticity: Transcription-dependent neuronal net-
766 work plasticity. The Journal of Physiology. 2005;564: 3–19. https://doi.org/10.1113/jphys-
767 iol.2004.077446 PMID: 15618268

768 73. Gullo F, Mazzetti S, Maffezzoli A, Dossi E, Lecchi M, Amadeo A, Krajewski J, Wanke E.
769 Orchestration of "presto" and "largo" synchrony in up-down activity of cortical networks.
770 Front Neural Circuits. 2010 Apr 22;4:11. https://doi.org/10.3389/fncir.2010.00011 PMID:
771 20461235

772 74. de la Peña E, Geijo-Barrientos E. Laminar Localization, Morphology, and Physiological
773 Properties of Pyramidal Neurons that Have the Low-Threshold Calcium Current in the

bioRxiv preprint doi: https://doi.org/10.1101/2022.04.05.487108; this version posted August 9, 2022. The copyright holder for this preprint (which was not certified by peer review) is the author/funder, who has granted bioRxiv a license to display the preprint in perpetuity. It is made available under aCC-BY-NC-ND 4.0 International license.

774 Guinea-Pig Medial Frontal Cortex. J Neurosci. 1996;16: 5301–5311.
775 https://doi.org/10.1523/JNEUROSCI.16-17-05301.1996 PMID: 8757243

776 75. Kawaguchi Y. Groupings of nonpyramidal and pyramidal cells with specific physiological
777 and morphological characteristics in rat frontal cortex. Journal of Neurophysiology.
778 1993;69: 416–431. https://doi.org/10.1152/jn.1993.69.2.416 PMID: 8459275

779 76. Sanchez-Vives MV, McCormick DA. Cellular and network mechanisms of rhythmic recur-
780 rent activity in neocortex. Nat Neurosci. 2000;3: 1027–1034. https://doi.org/10.1038/79848
781 PMID: 11017176

782 77. Winograd M, Destexhe A, Sanchez-Vives MV. Hyperpolarization-activated graded persis-
783 tent activity in the prefrontal cortex. Proceedings of the National Academy of Sciences.
784 2008;105: 7298–7303. https://doi.org/10.1073/pnas.0800360105 PMID: 18474856

785 78. Boehme R, Uebele VN, Renger JJ, Pedroarena C. Rebound excitation triggered by synaptic
786 inhibition in cerebellar nuclear neurons is suppressed by selective T-type calcium channel
787 block. Journal of Neurophysiology. 2011;106: 2653–2661.
788 https://doi.org/10.1152/jn.00612.2011 PMID: 21849607

789 79. Ferrante M, Shay CF, Tsuno Y, William Chapman G, Hasselmo ME. Post-Inhibitory Re-
790 bound Spikes in Rat Medial Entorhinal Layer II/III Principal Cells: In Vivo, In Vitro, and
791 Computational Modeling Characterization. Cereb Cortex. 2017 Mar 1;27(3):2111-2125.
792 https://doi.org/10.1093/cercor/bhw058 PMID: 26965902

793 80. Kurowski P, Grzelka K, Szulczyk P. Ionic Mechanism Underlying Rebound Depolarization
794 in Medial Prefrontal Cortex Pyramidal Neurons. Front Cell Neurosci. 2018;12: 93.
795 https://doi.org/10.3389/fncel.2018.00093 PMID: 29740284

796 81. Wu N, Enomoto A, Tanaka S, Hsiao CF, Nykamp DQ, Izhikevich E, et al. Persistent So-
797 dium Currents in Mesencephalic V Neurons Participate in Burst Generation and Control of
798 Membrane Excitability. Journal of Neurophysiology. mai 2005;93(5):2710-22.
799 https://doi.org/10.1152/jn.00636.2004 PMID: 15625100

800 82. Cui Y, Liu X, Yang T, Mei Y-A, Hu C. Exposure to extremely low-frequency electromag-
801 netic fields inhibits T-type calcium channels via AA/LTE4 signaling pathway. Cell Cal-
802 cium. 2014;55: 48–58. https://doi.org/10.1016/j.ceca.2013.11.002 PMID: 24360572

803 83. Pall ML. Electromagnetic fields act via activation of voltage-gated calcium channels to pro-
804 duce beneficial or adverse effects. J Cell Mol Med. 2013;17: 958–965.
805 https://doi.org/10.1111/jcmm.12088 PMID: 23802593

806 84. Wood A, Karipidis K. Radiofrequency Fields and Calcium Movements Into and Out of
807 Cells. Radiat Res. 2021 Jan 1;195(1):101-113. https://doi.org/10.1667/RADE-20-00101.1
808 PMID: 33206197

809 85. Sabatini BL, Regehr WG. Control of Neurotransmitter Release by Presynaptic Waveform
810 at the Granule Cell to Purkinje Cell Synapse. J Neurosci. 1997;17: 3425–3435.
811 https://doi.org/10.1523/JNEUROSCI.17-10-03425.1997 PMID: 9133368

bioRxiv preprint doi: https://doi.org/10.1101/2022.04.05.487108; this version posted August 9, 2022. The copyright holder for this preprint (which was not certified by peer review) is the author/funder, who has granted bioRxiv a license to display the preprint in perpetuity. It is made available under aCC-BY-NC-ND 4.0 International license.

812 86. Qian J, Saggau P. Modulation of Transmitter Release by Action Potential Duration at the
813 Hippocampal CA3-CA1 Synapse. Journal of Neurophysiology. 1999;81: 288–298.
814 https://doi.org/10.1152/jn.1999.81.1.288 PMID: 9914289

815 87. Kress GJ, Mennerick S. Action potential initiation and propagation: Upstream influences
816 on neurotransmission. Neuroscience. 2009;158: 211–222. https://doi.org/10.1016/j.neuro-
817 science.2008.03.021 PMID: 18472347

818 88. Ramezani H, Akan OB. Impacts of Spike Shape Variations on Synaptic Communication.
819 IEEE Trans.on Nanobioscience. 2018;17: 260–271.
820 https://doi.org/10.1109/TNB.2018.2838056 PMID: 29994535

821 89. Du J, Bradley RM. Effects of GABA on acutely isolated neurons from the gustatory zone
822 of the rat nucleus of the solitary tract. Chem Senses. 1998 Dec;23(6):683-8.
823 https://doi.org/10.1093/chemse/23.6.683 PMID: 9915114

824 90. Baufreton J, Garret M, Dovero S, Dufy B, Bioulac B, Taupignon A. Activation of GABA
825 A Receptors in Subthalamic Neurons In Vitro: Properties of Native Receptors and Inhibi-
826 tion Mechanisms. Journal of Neurophysiology. 2001;86: 75–85.
827 https://doi.org/10.1152/jn.2001.86.1.75 PMID: 11431489

828 91. Field AS, Ginsburg K, Lin JC. The effect of pulsed microwaves on passive electrical prop-
829 erties and interspike intervals of snail neurons. Bioelectromagnetics. 1993;14: 503–520.
830 https://doi.org/10.1002/bem.2250140603 PMID: 8297395

831 92. Volgushev M, Vidyasagar TR, Chistiakova M, Yousef T, Eysel UT. Membrane properties
832 and spike generation in rat visual cortical cells during reversible cooling. The Journal of
833 Physiology. 2000;522: 59–76. https://doi.org/10.1111/j.1469-7793.2000.0059m.x PMID:
834 10618152

835 93. Hedrick T, Waters J. Spiking patterns of neocortical L5 pyramidal neurons in vitro change
836 with temperature. Front Cell Neurosci. 2011 Jan 25;5:1.
837 https://doi.org/10.3389/fncel.2011.00001 PMID: 21286222

838 94. Goldin MA, Mindlin GB. Temperature manipulation of neuronal dynamics in a forebrain
839 motor control nucleus. Troyer TW, editor. PLoS Comput Biol. 2017;13: e1005699.
840 https://doi.org/10.1371/journal.pcbi.1005699 PMID: 28829769

841 95. Liu X, Qiao Z, Chai Y, Zhu Z, Wu K, Ji W, et al. Nonthermal and reversible control of
842 neuronal signaling and behavior by midinfrared stimulation. Proc Natl Acad Sci USA.
843 2021;118: e2015685118. https://doi.org/10.1073/pnas.2015685118 PMID: 33649213

844

845

846

847

bioRxiv preprint doi: https://doi.org/10.1101/2022.04.05.487108; this version posted August 9, 2022. The copyright holder for this preprint (which was not certified by peer review) is the author/funder, who has granted bioRxiv a license to display the preprint in perpetuity. It is made available under aCC-BY-NC-ND 4.0 International license.

848 # Supporting information

849 **S1 Table. Metrics definition: Analysis of neural network activity**

Analysis of neural network activity **Metrics**	
Day in vitro (DIV)	Age of the culture (in days) from preparation date (DIV_0) to recording date (DIV_n)
Active channel (k)	Number of channels showing both spiking and bursting activities
Mean spike rate (MSR)	Sum of channel mean spike rate (sec^{-1})
Mean burst rate (MBR)	Sum of channel mean burst rate (sec^{-1})
Network bursting rate (NtBR)	Rate of bursts occurring simultaneously in ≥ 20 channels (min^{-1})
% of spike outside bursts	Ratio of the number of spikes outside bursts to the total of number of spikes.
Mean Interburst interval (IBI)	Pooled mean of mean channel IBI (sec)
Mean Burst duration (BD)	Pooled mean of mean channel BD (msec)
Mean intraburst spike rate (IBSR)	Pooled mean of mean channel IBSR (n spike in burst / burst duration)*1000), Hz)
Coefficient of variation (CV)	Ratio (expressed in %) of the average channels standard deviation to the metric mean value (either IBI, BD or IBSR)
Initial inhibitory rate	Linear regression of 4 points over peri-exposure period, 2 min before exposure-onset and 2 min after exposure-onset
Postinhibitory rebound	Ratio between the maximal values (either MBR or MSR) retrieved in two consecutive non-overlapping windows of 4 min after exposure-offset

850
851
852
853
854
855
856
857
858

bioRxiv preprint doi: https://doi.org/10.1101/2022.04.05.487108; this version posted August 9, 2022. The copyright holder for this preprint (which was not certified by peer review) is the author/funder, who has granted bioRxiv a license to display the preprint in perpetuity. It is made available under aCC-BY-NC-ND 4.0 International license.

859 **S2 Table. Raw values at baseline of the various metrics used to describe neural networks**
860 **activity across the various experimental groups.**

Metrics	SH	RF	MU
N culture	12	15	8
N culture per animal	2 (3)	4 (3.5)	3 (1.5)
Day In Vitro	18.5 (1.5)	20 (2)	23 (2.5) *(2)
Active k	49 (13)	54 (6)	54 (5)
MSR (sec^{-1})	15.6 (18.5)	23.4 (37.3)	52 (43.2) *(2)
MBR (sec^{-1})	2.5 (2.6)	3.5 (2)	11.3 (12.7) *(2)
NtBR (min-1)	3.9 (5.3)	3.3 (1.6)	16.9 (16.4) *(2)
% of spike outside bursts	28.3 (21.9)	25 (21.5)	16.9 (12.3)
IBI (sec)	40.3 (35.6)	23.9 (11.8)	6.8 (10.5) *(2)
CV IBI (%)	19.3 (13.7)	17.4 (8.8)	8.8 (7.7) ns
BD (ms)	89 (102.5) *(1)	217 (91.8)	200.6 (115.4)
CV BD (%)	7 (3.4)	5.2 (3)	4.2 (1.8) *(2)
IBSR (Hz)	160.3 (46.9)	131.4 (42)	122 (35.9)
CV IBSR (%)	6.8 (3.9)	5.1 (2.1)	4.2 (2.3)

Data expressed as Median (IQR). *(1) Indicates significant difference between SH-RF and SH-MU pairs ($p < 0.05$) and *(2) indicates significant difference between MU-SH and MU-RF pairs ($p < 0.05$), ns indicates no significant differences between groups. Pairwise comparison done with Kruskal-Wallis test followed by Conover's all-pairs posthoc test. SH, n = 12; RF, n = 15; MU, n = 8.

861
862
863
864
865
866
867
868
869
870
871
872

bioRxiv preprint doi: https://doi.org/10.1101/2022.04.05.487108; this version posted August 9, 2022. The copyright holder for this preprint (which was not certified by peer review) is the author/funder, who has granted bioRxiv a license to display the preprint in perpetuity. It is made available under aCC-BY-NC-ND 4.0 International license.

873 **S1 Fig. AP detection, sorting, cluster repartition and waveform analysis**

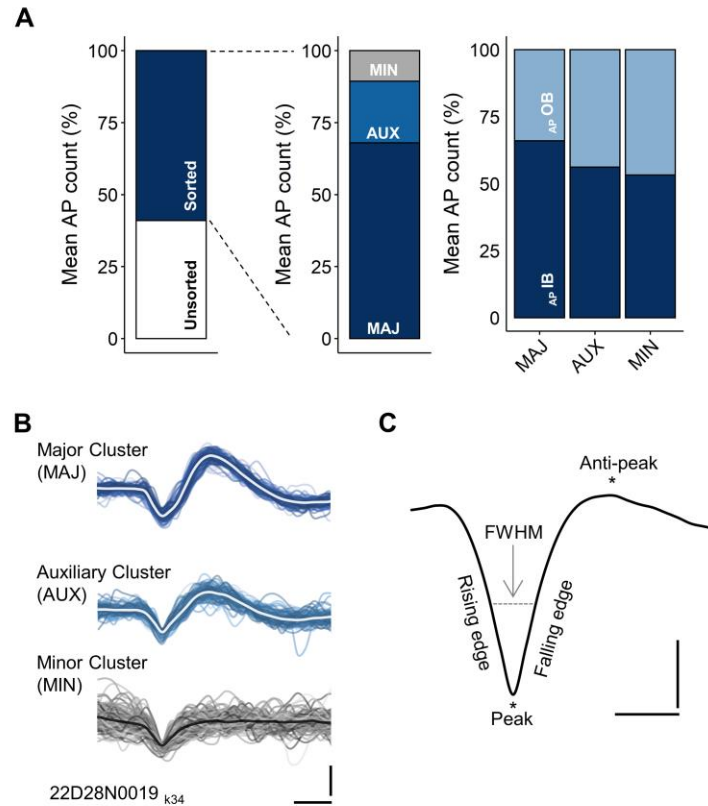

(A) From left to right: Mean AP detection for unsorted and sorted AP fraction (% of total detected APs); Relative fraction of sorted APs attributed to Major (MAJ), Auxiliary (AUX) and Minors (MIN) clusters; Mean AP count for sorted AP occurring either inside (AP IB) or outside (AP OB) bursts period. Data collected over 15 min during the pre-exposure phase from 15 cultures of the RF group used here as representative. **(B)** Example of sorted AP waveforms after principal component analysis and hierarchical classification, overlay of 125 waveforms per cluster with averaged waveform highlighted, data from one channel of a the same culture. Scale: (y): 40 µV; (x): 500 µs. **(C)** Illustration of the metrics used to quantify changes in AP waveforms. FWHM: full width at half maximum. As recorded extracellularly the AP waveform is inverted. Scale: (y): 10 µV; (x): 500 µs.

874
875
876
877
878
879
880
881

bioRxiv preprint doi: https://doi.org/10.1101/2022.04.05.487108; this version posted August 9, 2022. The copyright holder for this preprint (which was not certified by peer review) is the author/funder, who has granted bioRxiv a license to display the preprint in perpetuity. It is made available under aCC-BY-NC-ND 4.0 International license.

882 **S3 Table. Metrics definition: Analysis of AP waveform**

Analysis of spike waveform

Metrics	
Peak amplitude (µV)	Maximal amplitude of the first peak (negative going)
Anti-peak amplitude (µV)	Maximal amplitude of the second peak (positive going)
Half-width (µs)	Full width at half maximum (FWHM) of the first peak computed with linear interpolation
Rising edge (µV/ 10^{-01} ms)	Maximal slope of the AP rising edge (negative going)
Falling edge (µV/ 10^{-01} ms)	Maximal slope of the AP falling edge (positive going)

883

884 **S4 Table. Average raw values at baseline of the various metrics used to quantify change**
885 **in AP waveform across the various experimental groups**

Metrics	**SH**	**RF**	**MU**
Channel per MEA (count)	53 (12)	54 (6.5)	53 (2.3)
Sorted AP (count)	23 266 (18 327)	31 713 (17 353)	139 499 (87 694) *
Peak amplitude (µV)	-27.3 (11.1)	-28.9 (6.2)	-29.1 (5.7)
Anti-peak amplitude (µV)	11.2 (7.8)	13.1 (6.5)	15.3 (2)
Half-width (µs)	224.6 (39.7)	247.9 (29.8)	253.5 (52.3)
Rising edge (µV/ 10^{-01} ms)	-12.8 (5.7)	-13.7 (3)	-13.9 (4.8)
Falling edge (µV/ 10^{-01} ms)	12.8 (7.3)	14.6 (3.8)	15.21 (6)

Data expressed as Median (IQR). * Indicates significant difference ($p < 0.05$) between MU-SH and MU-RF pairs. Pairwise comparison done with Kruskal-Wallis test followed by Conover's all-pairs posthoc test. SH, n = 12; RF, n = 15; MU, n = 8.

886